Dosimetric effects of removing the flattening filter in radiotherapy treatment units

Dalaryd, Mårten

2015

Dosimetric effects of removing the flattening filter in radiotherapy treatment units

Mårten Dalaryd

LUND
UNIVERSITY

DOCTORAL DISSERTATION

Abstract

The aim of this work was to investigate the dosimetric effects of removing the flattening filter from conventional C-arm medical linear accelerators. In conventional linear accelerators used for radiotherapy, a flattening filter is positioned in the beam line to provide a uniform lateral dose profile at a specified depth in water. However, for some radiotherapy treatments, a uniform lateral dose profile is not necessary, e.g. stereotactic treatments with small fields or treatments with intensity modulated fields.

In this work, a comprehensive set of measurements and Monte Carlo simulations for a modified Elekta Prec*i*se linear accelerator, operating with and without a flattening filter, were performed and the differences were evaluated. For an Elekta Prec*i*se linac, it was found that by removing the flattening filter the dose could be delivered approximately twice as fast as when the flattening filter is in the beam line, under certain conditions. The scatter produced in the treatment head was reduced by 30 %–45 % when the flattening filter was removed and the variation of scattered radiation with field size was also reduced. Removal of the flattening filter resulted in a softer photon energy spectra which leads to a steeper absorbed dose fall-off with depth and less lateral variation across the field. By increasing the acceleration potential of the linac, the depth–dose profiles become more similar to those of the equivalent conventional photon beam and thus the output will also be increased.

The suitability of two beam quality measures, $TPR_{20,10}$ and $\%dd(10)_x$ in predicting water to air mass collision stopping-power ratios $s_{w,air}$ for flattening filter-free photon beams was also investigated. These quality measures are used in reference dosimetry for the determination of absorbed dose in water. It was shown that the relationship between $TPR_{20,10}$ and $s_{w,air}$ used in a current international code of practice for reference dosimetry, overestimates the stopping-power ratio by approximately 0.3 % for flattening filter-free photon beams, while the relationship between $\%dd(10)_x$ and $s_{w,air}$, used in the North American code of practice is more accurate. A new beam quality metric, consisting of both $TPR_{20,10}$ and $TPR_{10,5}$ was evaluated. It was found that this new beam quality specifier more accurately predicted stopping power ratios for flattening filter-free photon beams. A beam quality specifier defined by the first two moments (describing the mean and variance) of the spectral distribution was also investigated and found to accurately predict stopping-power ratios for beams without a flattening filter.

Summary in Swedish

Vid extern strålbehandling används en s.k. linjäraccelerator för att producera och leverera den önskade strålningen till cancertumörer. I linjäracceleratorn accelereras elektroner till nära ljusets hastighet och styrs sedan mot en metalplatta där de bromsas upp och genererar bromsstrålningsfotoner (högenergetisk röntgenstrålning). Intensiteten av den strålning som sänds ut är störst i den riktning som elektronerna haft, det vill säga mitt i det fält som genereras, och för att generera ett strålfält med lika hög intensitet överallt placeras ett konformat utjämningsfilter i strålfältet. Filtret ger dock upphov till vissa nackdelar och ett homogent strålfält är idag inte nödvändigt för att leverera vissa typer av strålbehandlingar.

I det här arbetet har egenskaper hos en linjäraccelerator utan utjämningsfilter undersökts. Istället för filtret placerades antingen en tunn koppar- eller järnplatta i strålfältet, vilket är en nödvändighet för att kunna kontrollera strålfältet på ett säkert sätt.

Mätningar och datorberäkningar med så kallad Monte Carlo-teknik, både av det nya strålfältet samt av konventionella strålfält med utjämningsfilter har genomförts, för att ta reda på vilka skillnader som finns i den levererade strålningen. Denna nya behandlingsteknik levererar strålningen med dubbelt så hög intensitet centralt i strålfältet, något som kan leda till kortare behandlingstider. Den ger också upphov till mindre spridd strålning och mindre transmission genom de metallblock som formar strålfältet, vilket kan minska onödig bestrålning av patienten.

Det har inte varit bekräftat hur väl man kan mäta den absorberade dosen från kliniska fotonfält utan utjämningsfilter enligt internationella rekommendationer för jonkammardosimetri. I detta arbete utvärderades hur väl en viktig parameter för dessa mätningar kan förutsägas när stålkvalitetsmått som främst är framtagna för fält med utjämningsfilter används för kliniska strålfält utan utjämningsfilter. Två nya stålkvalitetsmått undersöktes också, vilka visade sig vara mer noggranna än de som rekommenderas internationellt.

List of original papers

This thesis is based on studies reported in the following publications, which are referred to in the text by their roman numerals. The publications are appended at the end of the thesis.

I. **Dosimetric characteristics of 6 and 10MV unflattened photon beams.**
Kragl G, af Wetterstedt S, Knäusl B, Lind M*, McCavana P, Knöös T, McClean B, Georg D
Radiotherapy and Oncology 93: 141-146, 2009

II. **A Monte Carlo study of a flattening filter-free linear accelerator verified with measurements.**
Dalaryd M, Kragl G, Ceberg C, Georg D, McClean B, af Wetterstedt S, Wieslander E, Knöös T
Physics in Medicine and Biology 55: 7333-7344, 2010

III. **Prediction of stopping-power ratios in flattening-filter free beams.**
Ceberg C, Johnsson S, Lind M*, Knöös T
Medical Physics 37: 1164-1168, 2010

IV. **Combining tissue-phantom ratios to provide a beam-quality specifier for flattening filter free photon beams.**
Dalaryd M, Knöös T, Ceberg C
Medical Physics 41: 111716, 2014

The publications have been reproduced with the permission of the following publishers:

Elsevier Inc. (**Paper I**)
Institute of Physics Publishing Ltd (**Paper II**)
American Association of Physicists in Medicine (**Papers III and IV**)

* Mårten Lind changed his name to Mårten Dalaryd in May 2010.

List of contributions

Paper I – I planned and performed measurements, and participated in the analysis and the preparation of the manuscript.

Paper II – I planned, prepared and conducted the experiment. I performed the data analysis and was the main author of the publication.

Paper III – I performed preparatory Monte Carlo calculations, and participated in the analysis and the preparation of the manuscript

Paper IV – I planned, prepared and conducted the experiment. I performed the data analysis and was the main author of the publication.

Reports have been presented at the following international meetings

i. The NACP 2008 Symposium, Aarhus, Denmark, 2008 (<u>Lind M</u>, Wieslander E, McClean B, McCavana P, Knöös T, Characteristics of a Flattening Filter Free Photon beam –measurements and Monte Carlo simulations)

ii. MCTP 2009, Cardiff, Wales, 2009 (<u>Lind M</u>, Wieslander E, af Wetterstedt S, Knöös T, McClean B, McCavana P, Georg D and Kragl G, Characteristics of a Flattening Filter Free Photon beam –measurements and Monte Carlo simulations)

iii. The 10th Biennial ESTRO Meeting, Maastricht, Netherlands, 2009 (<u>Lind M</u>, Knöös T, Ceberg C, Wieslander E, McClean B and Georg D, Photon beam characteristics at monitor chamber level in a flattening filter free linac: a Monte Carlo study *Radiother. Oncol.* **92** (suppl 1) S57)

iv. The 31st Annual ESTRO Meeting, Barcelona, Spain, 2012 (<u>Dalaryd M</u>, Ceberg C, Knöös T, A 2D beam-quality specifier for flattening filter free beams *Radiother. Oncol.* **103** (suppl 1) S86)

Publications not included in this thesis

Flattening filter free beams in SBRT and IMRT: dosimetric assessment of peripheral doses.
Kragl G, Baier F, Lutz S, Albrich D, <u>Dalaryd M</u>, Kroupa B, Wiezorek T, Knöös T, Georg D.
Zeitschrift für Medizinische Physik 21: 91-101, 2011

Contents

1 Background

1.1 The Medical Linear Accelerator

For approximately half of all cancer patients in Sweden, radiotherapy is recommended at some stage in their treatments (Nyström and Thwaites, 2008) and the linear electron accelerator (linac) is by far the most common equipment for this delivery. In the following section, a general overview of the common design principles of a modern linac is presented, although individual vendors differ in how specific details are implemented.

By heating a tungsten filament (the electron 'gun'), electrons are liberated and then accelerated using radio frequency fields within a waveguide close to the speed of light. For conventional C-arm linacs, the accelerator gantry needs to be able to rotate around the patient; the geometry of the accelerator structure is constrained to be horizontal, with bending magnets used to redirect the electron beam through approximately 90° and thus directed vertically down to the patient positioned on a treatment table. High-energy bremsstrahlung X-ray photons are generated by directing the electron beam through a target of sufficiently high atomic number, usually tungsten. These photons are then collimated by a primary collimator.

In the typical clinical energy range (4 MV–25 MV accelerating potential), the angular distribution of the bremsstrahlung photons is predominantly in the direction of the incident electrons. This distribution is further modified by a so called 'flattening' filter (FF), designed to give an almost uniform lateral dose distribution to the patient at a specific treatment depth, typically 10 cm.

In modern clinical linear accelerators these filters consist of conical shaped pieces of metal, typically made of medium- and/or high-Z materials such as iron, copper or tungsten, and are specific to each particular beam energy. The central part of these filters can be several centimetres thick (Izewska, 1993). The filters are usually mounted on a rotating carousel so that the appropriate filter can be positioned in the photon beam. In some machines a combination of filters is needed, and in these cases the rotating carousel filter is combined with a fixed filter positioned at the end of the primary collimator.

Below ('after' in the direction of the propagating radiation) the flattening filter(s), two independent transmission ion chamber arrays provide servo control of beam steering and dose output, while also providing a level of redundancy in patient safety due to misaligned beams or excessive radiation output. The final shape of the beam is further collimated by the moveable beam aperture located just above the exit window of the treatment head. Two pairs of opposing 'jaws' limit the field size in orthogonal directions, and conformation to a target shape is further improved by multi-leaf collimators (MLC), consisting of between 40 and 160 individual tungsten 'leaves' which can be individually positioned to shield healthy tissue surrounding the treatment target. Figure 1.1 shows a schematic diagram illustrating the main components within the treatment head on an Elekta linac (Elekta Oncology Systems, Stockholm, Sweden).
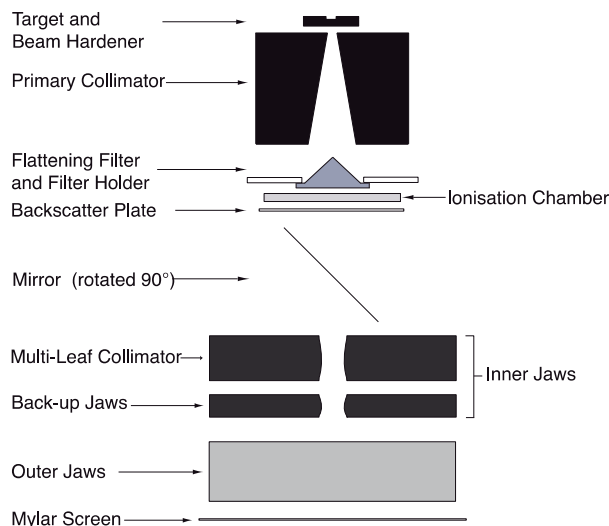
Figure 1.1. Schematic illustration of the components in an Elekta linac head (not to scale) (Adopted from **Paper II**).

1.1.2 The flattening filter

Flattening filters have been standard in medical linear accelerator design since the 1950's but there are disadvantages regarding their use. To ensure a uniform intensity profile across the whole extent of the beam, a large fraction of beam intensity at the central axis is removed thus decreasing the total output of the machine while at the same time generating scattered radiation (Petti *et al.*, 1983; Zhu and Bjarngard, 1995). This scattered radiation (comprising of both photon and electron components)

contributes to undesirable dose to the patient and can be difficult to model accurately in radiotherapy treatment planning systems (TPS).

Photons penetrating the flattening filter are subjected to a differential amount of absorption depending on which point of the filter they pass through, leading to increased 'softening' of the beam energy away from the central axis as reported via Monte Carlo (MC) calculations (McCall *et al.*, 1978). Mohan *et al.* (1985) used an improved model of a linac to show that for a 6 MV clinical beam measured isocentrically (100 cm from the effective radiation source), the average photon energy is reduced from 1.92 MeV on-axis to 1.51 MeV in an annular region 15 cm to 20 cm off-axis. The same study also described the off-axis softening effect as a decrease in the half-value layer (HVL) thickness with increasing off-axis distance. A consequence of the non-uniform spectral composition laterally within the beam is the resultant non-uniform lateral attenuation of the beam; a well-known effect of this is the presence of so-called 'horns' on lateral dose profiles measured at depths shallower than the specified reference depth, as illustrated in Figure 1.2.
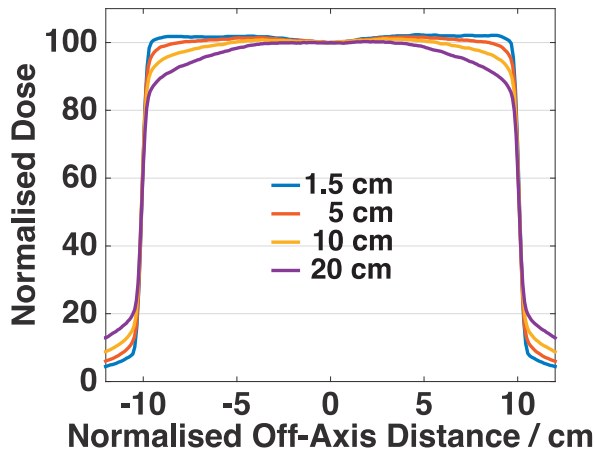
Figure 1.2. Lateral beam profiles for the same photon beam at different depth with fixed source-to-surface distance. The divergence of the beam has been removed by renormalising the off-axis distance and all beams are normalised to the dose at the central axis.

Because of the beam hardening (removal of lower energy photons), the relative reduction in fluence on axis, and the increased scatter from the filter, there is an increase in radiation leakage through the shielding and a subsequent increase in out of field dose (Almberg *et al.*, 2012; Kry *et al.*, 2010; O'Brien *et al.*, 1991). Additionally, for photon beam energies above the threshold for photonuclear reactions (~10 MV), the flattening

filter is one of the components in which this reaction occurs. Monte Carlo studies for an 18 MV photon beam from Varian accelerators has shown that the flattening filter is responsible for roughly 10 % of the neutron production in the treatment head (Kry *et al.*, 2007; Zanini *et al.*, 2004). This figure is dependent on the material of the flattening filter.

1.2 Removal of the flattening filter

Early studies investigated the characteristics of 'unflattened' beams compared to those produced conventionally with a flattening filter. A previously mentioned study (Mohan *et al.*, 1985) showed that without a filter (or collimating system), the average photon energies in a 15 MV clinical beam, measured isocentrically, only varied from 2.8 MeV at the central axis to 2.5 MeV in an annular region 10 cm to 25 cm off-axis, whereas for the same beam in a conventionally flattened and collimated system, the mean energies were 4.11 MeV on axis, and 3.3 MeV off axis, respectively. Other studies investigated the effect on the depth of maximum dose (Sixel and Podgorsak, 1994), spectral changes at off-axis positions (Zefkili *et al.*, 1994) and head scatter (Zhu and Bjarngard, 1995).

The main reason why flattening filter-free (FFF) beams have not been used historically is the forward peaked dose distribution. One of the earliest studies investigating the impact on treatment delivery following the removal of the flattening filter from a conventional linac was O'Brien *et al.* (1991) which looked at the reduction in treatment delivery time for stereotactic body radiotherapy (SBRT) and was facilitated by physically removing the flattening filter from the treatment head of a Therac-6 linac (Atomic Energy of Canada Ltd., Mississauga, Ontario, Canada). The treatment beam-on time for a 25 Gy fraction was reduced from ~15 minutes to ~7 minutes with a 15 %–50 % reduction in dose to critical organs outside the treatment volume. A follow up study on the same linac investigated changes in the photon spectra (Sixel and Faddegon, 1995).

Stereotactic treatments were initially the main focus of research initially because the smaller field sizes were less affected by the lateral dose fall-off. For instance, O'Brien *et al.* (1991) reported doses of 95 % of the central axis dose measured 2.5 cm off axis. However, the advent of modern radiotherapy TPS presented the opportunity to shape the required photon fluence needed for treatment delivery regardless of the fluence exiting the collimating system, by modulating the treatment fields.

In a Chinese study from 2004 the delivery time for intensity modulated radiotherapy (IMRT) treatments were investigated with and without a flattening filter (Fu *et al.*, 2004). In this semi-theoretical study, the flattening filter was removed from a BJ-6B

linear accelerator (Beijing Medical Equipment Institute, Beijing) and beam data for the treatment planning system was collected. However, the accelerator was not equipped with an MLC and it was later added only in the TPS models. The beam on times were then calculated based on the resulting MLC movements and monitor units required to deliver the IMRT-treatments and they found a 43 % decrease in beam-on time when the flattening filter was removed, while still meeting the dose prescribed to the target and dose constraints on the risk organs.

In 2006, a group at MD Anderson Cancer Center (Huston, USA) began publishing a series of studies on flattening filter-free photon beams delivered by Varian linear accelerators (Varian Medical Systems, Palo Alto, USA) (Kry *et al.*, 2009; Kry *et al.*, 2008; Kry *et al.*, 2007; Kry *et al.*, 2010; Ponisch *et al.*, 2006; Titt *et al.*, 2006a; Titt *et al.*, 2006b; Vassiliev *et al.*, 2009; Vassiliev *et al.*, 2007; Vassiliev *et al.*, 2006a; Vassiliev *et al.*, 2006b; Zhu *et al.*, 2006). These studies can be seen as the starting point of a period of intense publishing on flattening filter-free photon beams delivered by conventional linacs.

1.2.1 Replacement filter

Titt *et al.* (2006a) found through Monte Carlo simulations that an excessive amount of contaminating electrons were exiting the linac when the flattening filter was removed from a Varian Clinac 2100 accelerator. A large portion of these electrons had passed through the target and by inserting a thin Copper foil in the beam line it was shown that many of these electrons were absorbed, along with some of the lower-energy photons. Varian later released their 'TrueBeam' unit with flattening filter-free capability in 2010, which included a replacement filter consisting of 0.8 mm brass. Cashmore (2008) argued that the lack of scattered electrons from the flattening filter must be compensated for when operated in FFF-mode. In particular, he found that replacing the flattening filter with a homogeneous metal disk would provide enough signal in the ion monitor chambers needed for the steering servos. When Elekta released a flattening filter-free beam mode as a research option, they decided to use a 6 mm copper filter as a replacement for the flattening filter. This filter was included in the beams investigated in **Papers I** and **II,** since at that time this was the only replacement filter the manufacturer could provide. We also included this filter in **Paper IV** to study the effect on stopping power ratios when different replacement filters were used. A thinner filter consisting of 2 mm stainless steel was also investigated (**Paper IV**) since this filter is used in the current clinical linac with FFF ability from Elekta (Xiao *et al.*, 2015).

At the time of publishing **Paper I**, no measurement study describing the dosimetric effect of replacing the flattening filter with a 6 mm Cu plate on an Elekta linac had been performed. There were also no previous measurements on a 10 MV FFF beam for

this model of linac. Cashmore (2008) did investigate if the surface dose was affected when different plates of Al and Cu (1.1 and 1.9 mm Al; 1.9 mm Cu) were used as a replacement for the flattening filter but no significant differences were found. It was not stated in the article that the measured flattening filter-free data presented in the study was acquired with a replacement filter. In the publication it was stated that in flattening filter-free mode the filter carousel was rotated so that the beam passed through an "open" port. However, this "open" port was not entirely open but contained a 2 mm thick aluminium plate (Cashmore, 2013).

Monte Carlo simulations of an Elekta SL 25 linac operating in flattening filter-free mode were published in 2007 and 2008 (Mesbahi, 2009; Mesbahi *et al.*, 2007; Mesbahi and Nejad, 2008). However, in the simulation of flattening filter-free beams, no replacement filter was included.

Even though Siemens (Siemens, Erlangen, Germany) no longer produces commercial clinical accelerators, they did develop a flattening filter-free beam with a 1.27 mm aluminium replacement filter (Xiao *et al.*, 2015).

1.2.2 Other flattening filter-free treatment devices

Some treatment devices specifically designed for delivery of intensity modulated radiotherapy (IMRT) are not equipped with a flattening filter.

The CyberKnife linac (Accuray Incorporated, Sunnyvale, USA) is mounted on a robotic arm and delivers small circular fields with a diameter ranging from 5 mm to 60 mm at an source-to-surface distance (SSD) of 80 cm. The treatment is delivered though hundreds of individual fields by repositioning the unit using the robotic arm (Adler *et al.*, 1997). In this unit, the flattening filter has been replaced with what is called an electron filter, i.e. a flat metal plate made of lead.

In intensity modulated arc therapy (IMAT), a form of IMRT, the radiation source (linac) continuously delivers radiation while rotating around the patient. The TomoTherapy unit (Accuray Incorporated, Sunnyvale, USA) is dedicated for IMAT delivery and it has a delivery technique similar to how Computer Tomography (CT) imaging is performed (Mackie *et al.*, 1993). In TomoTherapy machines the linac is mounted on a rotating disc. The radiation field is collimated by a binary MLC combined with motorised jaws with three different field width positions (maximum field size is 5 cm x 40 cm). A fan beam is continuously delivered in a helical arc by rotating the linac and the treatment couch is moved through the radiation field, with the modulation achieved by switching individual MLC leaves in and out. With this modality the flattening filter is not necessary and has been replaced by a flat beam hardener (Jeraj *et al.*, 2004).

The MM50 racetrack microtron proposed in the 1980s is a radiotherapy unit lacking a flattening filter, but still producing a flat photon beam. This is achieved by scanning the incident electron beam on a thinner target plate (Brahme *et al.*, 1980; Karlsson *et al.*, 1988). In principle this technique could also be used for scanned photon beam IMRT, where the intensity modulation is performed by the scanning pattern of the incident electron beam rather than the collimating structures.

1.3 Accuracy required in external beam radiation therapy

In radiotherapy there are high demands on accurate determination of the delivered dose to the patient. Both tumour and healthy tissues are affected by ionising radiation but their biological responses differ. The relationship between biological effect and absorbed dose is generally described by sigmoidal dose–effect curves for both tumour and healthy tissue. Accurate dose delivery is important, ensuring the delivered dose is within the narrow 'therapeutic window' maximising the probability for tumour control while minimising the surrounding normal tissue complications. In Report 24 of the International Commission on Radiation Units and Measurements (ICRU) it is recommended that the delivered dose to the target needs to be accurate within ±5 %[1], based on clinical observations for certain tumour types (ICRU, 1976). It is also stated that some clinicians proposed a limit as small as 2 % but at that time (1976) it was considered virtually impossible. The lowest dose differences clinically detectable are reported to be in the order of ±5 % – ±10 % according to the International Commission on Radiological Protection (ICRP, 2000). Other studies have proposed accuracy requirements in the delivered dose to the patient in the order of 3 %–3.5 % (1 SD) (Brahme *et al.*, 1988; Mijnheer *et al.*, 1987). To arrive at an accuracy as low as 3 %–5 % (1 SD) in the delivered dose to the patient is a challenging task considering the complexity of the radiotherapy chain and obviously requires that uncertainties in all parts of this chain are as low as possible.

Updating the uncertainty analysis by Ahnesjö and Aspradakis (1999) with the latest estimation of dose determination (Andreo *et al.*, 2000) we will get an overall uncertainty in absorbed dose to the patient of 3.9 % (1 SD) (excluding uncertainties in the dose calculation in the TPS). The uncertainty component of the determination of absorbed dose at the calibration included in this figure is estimated to be 1.5 % (1 SD) and in Table 39 of Andreo *et al.* (2000) this uncertainty level requires that the assignment of stopping-power ratios to beam quality is as low as 0.2 % (1 SD).

---

[1] It was not explicitly stated by the ICRU what this figure represented (e.i. range, 1 SD).

1.4 Aims of the work

The overall aim of the work presented in this thesis was to investigate the dosimetric effects following the removal of the flattening filter from a medical linear accelerator.

The first aim was to evaluate basic dosimetric properties of flattening filter-free photon beams and to compare with conventionally flattened photon beams delivered by an Elekta Precise linear accelerator operating at 6 MV and 10 MV. The specific goals were:

- Characterisation of measurable dosimetric properties of flattening filter-free photon beams (**Paper I**).

- Use Monte Carlo methods to characterise unmeasurable effects of removing the flattening filter (**Paper II**).

The second aim was to investigate the relationship between different beam quality metrics and Spencer-Attix restricted water-to-air mass collision stopping-power ratios for flattening filter-free photon beams. The specific goals of this part were:

- Investigate the feasibility of using a more general beam-quality specifier based on the kerma-weighted mean, and the coefficient of variation of the linear attenuation coefficient in water of flattening filter-free photon beams (**Paper III**).

- Evaluate the accuracy in reference dosimetry for flattening filter-free photon beams using international dosimetry protocols (**Paper IV**).

- Investigate an additional parameter for improving reference dosimetry (**Paper IV**).

2 The Monte Carlo method

2.1 Introduction

A general description of the Monte Carlo method is that it offers a solution to a macroscopic system through simulation of its microscopic interactions (Bielajew, 2013). It is a useful technique for a wide variety of situations with a complex structure of probabilistic nature, e.g. radiation transport in matter, where analytical approaches can be inadequate. MC is used as a numerical technique to simulate the individual trajectory of each particle by using (pseudo)random numbers to sample from the statistical distribution of the physical processes involved. The probability distributions used are derived from the underlying physical properties of the processes.

In order to achieve a prediction of the radiometric quantities of interest with high statistical accuracy a large number of histories (source particles) must be simulated. The overall accuracy in the estimate also depends on the accuracy of the underlying physical theories, interaction cross sections and the random number sequence, but also user input, such as the geometric modelling of the problem and parameters set by the user.

Monte Carlo methods are used for a broad range of applications in radiation therapy physics. Specific areas of interest are radiation dosimetry, treatment planning, quality assurance (QA) and design of the treatment devices (Andreo, 1991; Rogers, 2006; Seco and Verhaegen, 2013). The Monte Carlo method can provide information that cannot be obtained by other techniques such as measurement or analytical methods, e.g. where scattered radiation originates. In this work the Monte Carlo technique has been used to investigate dosimetric issues relating to reference dosimetry, namely how the relationship between stopping power ratios relates to common measures of beam quality, and how basic dosimetric properties are affected by the removal of the flattening filter.

2.2 Particle transport

When high-energy photons travel through a medium they undergo only a few interactions, since their mean free path is relatively large (in the order of decimetres in water). This range is of the same order of magnitude as the simulation geometry in radiotherapy physics and each individual event can therefore be simulated according to the relevant probability distribution (Rogers and Bielajew, 1990).

A more complex situation occurs when simulating the transport of electrons and positrons through matter because of the much larger number of interactions they undergo as they slow down. To simulate each and every such event is unfeasible as it would be extremely time consuming. Since almost all of the interactions are elastic or semi-elastic, the energy transfer to the surrounding medium for each interaction is either small or vanishingly small, and the majority of the scattering angles are also small. This enables a large number of individual electron interactions to be grouped together into a single condensed electron step. This technique was first introduced by Berger in 1963 and is called the condensed history (CH) technique (Berger, 1963). The energy loss and angular deflection of an electron for a condensed history step is sampled from probability distributions based on multiple scatter theories. For what is called a Class II CH scheme, "catastrophic" events, i.e. bremsstrahlung and δ-ray production, which occur above user specified energy thresholds, are simulated explicitly along with any resulting secondary particles.

2.3 General Purpose Monte Carlo codes

There are a number of Monte Carlo codes that can be used for simulations in radiotherapy physics applications. Examples of these are EGS, MCNP, GEANT and PENELOPE, all of which include a coupled electron–photon transport algorithm but with slight variations in the transport algorithms and in geometry and scoring definitions. In this work all simulations were performed using EGSnrc (Electron-Gamma-Shower)(Kawrakow, 2000a; Kawrakow *et al.*, 2011) which is a code developed from EGS4 (Nelson *et al.*, 1985). EGSnrc is the most widely used general purpose Monte Carlo code in the field of medical physics (Rogers, 2006), and has been extensively benchmarked, e.g. using the Fano test[2] showing that the ion-chamber

---

[2] This test is based on the validity of the Fano theorem stating that, in conditions of charged particle equilibrium, the electron fluence differential in energy is independent of density variations from point to point. The test can be used to benchmark the coupled electron-photon transport implementation in a Monte Carlo code.

response could be calculated within 0.1 % with respect to its own cross sections (Kawrakow, 2000b). EGSnrc has also been used in calculating Spencer-Attix water-to-air restricted mass collision stopping-power ratios used in current dosimetry protocols, e.g. International Atomic Energy Agency (IAEA) TRS-398 and American Association of Physicists in Medicine (AAPM) TG-51 (Ding *et al.*, 1995; Rogers and Yang, 1999).

Electron transport in EGSnrc is based on Goudsmit-Saunderson multiple scattering theory. The electron-step algorithm PRESTA II together with the EXACT boundary-crossing algorithm provides an advanced solution where the electron transport switches from multiple scatter to single scattering when electrons are within a user defined distance to boundaries, thereby avoiding step-size artefacts (Kawrakow *et al.*, 2011). As previously mentioned, a condensed history technique is used and energy losses along an electron step are grouped in such a manner that the energy is considered to be deposited evenly along this step, i.e. the electron step size is defined by the stopping power value according to the continuous slowing down approximation (CSDA). In class II electron transport algorithms, such as in EGSnrc, the CSDA is modelled by the restricted stopping power. The energy deposition along the electron step will be modelled by the restricted stopping power as long as the energies of bremsstrahlung photons and δ-rays are below the user defined threshold energies, AP and AE, respectively. All energy losses below these thresholds will be deposited evenly along the electron step and energy losses above the threshold energies will be modelled separately (Rogers and Bielajew, 1990).

2.4 Specific Purpose Monte Carlo codes

In the EGSnrc package there are several user codes for which EGSnrc handles the back-end physics of the radiation transport while the user codes handle geometry specifications and scoring of quantities of interest. In this work, several different user codes have been employed. Due to the continuous updating of the EGSnrc-package different versions have been used (v4-r2-3-0: **Paper II**, v4-r2-3-2: **Paper IV**) The user code BEAMnrc (Rogers *et al.*, 1995; Rogers *et al.*, 2011b) was developed for simulations of the treatment head of a medical linear accelerator and has been used extensively in this work (**Papers II**, **III** and **IV**). In BEAMnrc each vital structure of the linac head can be accurately modelled through the use of dedicated component modules. The interaction history of each primary incident electron and its secondary particles can be traced via the LATCH variable. Thus, when a large number of particles are simulated, information about the fraction of particles that interacted in a specific region can be obtained (Rogers *et al.*, 1995). This data can be stored in a so-called phase space file, together with information of energy, position, direction, charge, multiple crossings, etc. for every particle that crosses user specified planes in the model. This file

can then be used either for analysis or as an input source in a water tank simulation, for example. The dose distribution in the water tank can be simulated in a Cartesian voxelised geometry using DOSXYZnrc (Walters *et al.*, 2007) (**Paper II**) or in a cylindrical geometry with DOSRZnrc (Rogers *et al.*, 2011a) (**Paper IV**). For calculations of Spencer-Attix restricted mass collision stopping power ratios the user code SPRRZnrc (Rogers *et al.*, 2011a) has been used (**Paper IV**).

2.5 Variance Reduction Methods

MC simulations attempting to simulate the full stochastic development of radiation transport through the simulated accelerator head can, if a low variance is requested, be very time consuming. To estimate statistical uncertainties of the calculated results, a history-by-history method implemented by (Walters *et al.*, 2002) is used. The uncertainty is calculated using the standard error formula:

$$s_{\bar{X}}^2 = \frac{1}{N-1}\left[\frac{\sum_{i=1}^{N} X_i^2}{N} - \left(\frac{\sum_{i=1}^{N} X_i}{N}\right)^2\right] \tag{2.1}$$

where X_i is the quantity of interest scored in statistically independent history i and N is the number of independent histories, i.e. the number of initial particles. Since the uncertainty is estimated by grouping all events from the same primary particle, correlations between particles in a phase space source are accounted for. Variance reduction techniques decrease the calculation time by modifying the algorithm while maintaining an unbiased deviation from a comparative simulation performed without variance reduction (Fippel, 2013). In this section, only variance reduction methods used in this thesis are described. These fall into one of two broad categories, approximate variance reduction techniques ('enhancing' methods) which use various approximations in the physics to achieve a higher computational efficiency, and true variance reduction (such as bremsstrahlung splitting) which increase the efficiency without substantially changing the underlying physics in the model.

2.5.1 Cut-off Energies

The use of energy thresholds is one such approximation technique. A particle with energy below the cut-off threshold is 'terminated' and the remaining energy is deposited locally (Rogers *et al.*, 2011b). As previously mentioned one can also set threshold

energies for the production of bremsstrahlung photons and secondary electrons, AP and AE.

2.5.2 Range Rejection

The concept of range rejection is to terminate charged particles if their residual ranges are too small to leave a certain region. The range and distance to the nearest boundary are already calculated by the EGSnrc code for every electron step and the use of range rejection can save a large amount of calculation time. The pre-calculated electron range is set conservatively as it is calculated as the path length travelled until reaching the cut-off energy without any discrete interactions (Rogers *et al.*, 1995). This technique also involves a physical approximation since potential bremsstrahlung photons generated by the charged particles are ignored. An energy threshold, above which range rejection is not allowed, is defined to control the extent of this approximation. In regions where the bremsstrahlung process is an important interaction mechanism, e.g. in the target of a medical linear accelerator, range rejection must be turned off.

2.5.3 Bremsstrahlung Splitting and Russian Roulette

In order to increase the simulated bremsstrahlung production in the target, BEAMnrc offers different bremsstrahlung splitting techniques of which two have been used in this work: uniform (UBS) and directional (DBS) bremsstrahlung splitting.

Uniform Bremsstrahlung Splitting

When a bremsstrahlung event occurs, the number of photons emitted is increased by a number, *Ns,* and each photon is given a weight equal to 1/*Ns* times the weight of the electron that generated them. Each generated photon is given an energy and direction based on relevant probability distributions and are then transported individually. The energy of the photon-generating electron is reduced by the energy of just one of the photons to accurately preserve energy loss straggling of the electron. The consequence of this is that energy is not conserved for each history. Absolute conservation of energy would demand that the electron energy is decremented by the average energy of the photons. However, for a large number of splitting events, energy will, on average, be conserved (Rogers *et al.*, 2011b). This technique was employed for generation of some of the phase space files used for beam analysis presented in **Paper II** and the stopping power calculations presented in **Paper IV**.

Directional Bremsstrahlung Splitting

In Directional Bremsstrahlung Splitting (Kawrakow *et al.*, 2004), splitting is conducted with a fixed splitting number as in UBS. Then, photons aimed at a user specified region of interest (ROI) are always transported while photons aimed outside of this region undergo Russian Roulette with a survival probability of 1/Ns. Surviving photons (for which the random number in the Russian Roulette is less than 1/Ns) are given a statistical weight of 1 leading to all photons with directions inside the ROI having a weight of 1/Ns and those aimed outside having a statistical weight of one. The algorithm is also designed such that there are only few electrons reaching the plane of interest and they all have a weight equal to 1. In order to improve the statistics of contaminating electrons, there is an option of introducing a splitting plane for charged particles at which electrons are split Ns times (and have their weight reduced by a factor 1/Ns). The user can also select a plane where particles interacting below it are subjected to a more "relaxed" DBS algorithm than above it. Here, low-weight photons are allowed to interact normally when they undergo Compton scattering, pair production or photoelectric events. Charged particles generated by high-weight photons will be split Ns times (2×Ns for a pair production event). Electrons generated through Compton interaction of high weight photons are not subjected to Russian Roulette, as they would above the splitting plane. DBS was employed in accelerator simulations used for depth–dose and off-axis profiles presented in **Paper II** and **IV**.

2.6 Simulation of Linear Accelerators

For the studies presented in this thesis the entire linac head has been simulated for two different accelerators, the Elekta Prec*i*se and Elekta Synergy. Through a research agreement with the manufacturer, geometrical specifications of the different components were acquired. Since the validity of many of the geometrical and material specifications provided by the manufacturer cannot be experimentally determined, they are often regarded as the truth. Some parameters, such as the density of the collimators can be verified by simulations, but others, such as the flattening filter, rely on the information provided. Therefore it is of importance that the manufacturers make sure their specifications are correct. For instance, it has been shown that the density of the flattening filter can have a large impact on the calculated off-axis factors (Sheikh-Bagheri and Rogers, 2002).

A phase space can be tallied at a user defined source-to-surface distance, which can be used in a subsequent dose calculation (**Paper II and IV**), extracting beam properties (**Paper II**) and for calculations of Spencer-Attix mass-restricted stopping-power ratios (**Paper IV**).

Some vendors have decided to classify the full description of the components in the accelerator head and instead provide phase space information at a position just above the jaws. The user can then transport the particles in the phase space file through the collimating system but are unable to modify the electron beam striking the target. There is also the possibility to download phase space files, provided by the scientific community, from an IAEA website[3]. Phase space files provided by the vendor and downloaded from IAEA were used for calculating beam quality and stopping-power ratios for a Varian TrueBeam and an Elekta Prec*i*se linac (**Paper IV**). There were two reasons for this; firstly it was the only option, at the time, for one of the machines (Varian TrueBeam) since the proprietary geometrical information was not available; secondly, the use of an independent previously published model to test the proposed beam quality specifier. More recently, a reverse-engineered model of the TrueBeam linac head has been developed (Rodriguez *et al.*, 2015). In this model the geometry of a Clinac 2100 was modified in a trial-and-error process until simulated dose distributions agreed with measurements for a TrueBeam unit. However, for the purpose of **Paper IV**, the published phase-space files were considered to be more appropriate because of the uncertainty in the replacement filter used in the work by Rodriguez *et al.* (2015).

2.6.1 Tuning of the initial electron beam

The least known property of a Monte Carlo model of a medical linear accelerator involves the parameters of the electron beam incident on the target. The parameters to be determined are the mean energy, energy spread, spot size, and angular divergence of the electron beam. Some accelerator vendors provide information on the electron beam incident on the target. However, this information is generally uncertain and can only be regarded as an initial estimate (Sheikh-Bagheri and Rogers, 2002).

In order to commission a linac model, measurable quantities are compared to their corresponding calculated values. There are several publications with slightly different approaches on how to perform this validation and source tuning and no general consensus exists in the literature around the subject (Sawkey and Faddegon, 2009; Sheikh-Bagheri and Rogers, 2002; Tonkopi *et al.*, 2005; Tzedakis *et al.*, 2004; Verhaegen and Seuntjens, 2003).

The spot size of the electron beam can be measured (Verhaegen and Seuntjens, 2003). However it is a method requiring equipment not readily available in medical physics departments. The size and shape of the focal spot varies from machine to machine but were mostly found to have an ellipsoid shape (Verhaegen and Seuntjens, 2003).

---

[3] https://www-nds.iaea.org/phsp

Verhaegen and Seuntjens (2003) proposed a method consisting of three steps. First the energy of the electron beam should be determined by matching measured and calculated depth–dose profiles in water for a 10×10 cm^2 field. The second step involves comparisons of lateral dose profiles for larger fields to acquire the spot size parameter and the final step would be recalculation of depth–dose profiles when including the spot size parameter obtained in the second step.

It has also been suggested to use off-axis factors measured in air together with central-axis depth–dose curves for a Siemens KD linac (Sheikh-Bagheri and Rogers, 2002). It was shown that this procedure was sensitive to the mean energy and radial intensity distribution of the electron beam. However the energy spread showed no dependence on in-air off-axis ratios when the full width half maximum (FWHM) of a Gaussian energy distribution was varied between 0 % and 20 %. Since the depth–dose profiles only showed a weak dependence on the energy distribution it was concluded that the energy spread should be modelled as specified by the manufacturer.

Sheikh-Bagheri and Rogers (2002) could not find any variation of in-air off-axis ratios for an angular divergence below 0.5° and a variation of up to 5° did not affect the depth–dose profiles. Based on these findings and the fact that the manufacturer did not provide any reliable estimate, they ignored the angular divergence. Others have suggested including the angular dependence only if a match with measurement could not be achieved by varying the incident electron energy and spot size (Tonkopi *et al.*, 2005).

In a study on an Elekta SL75/5 the electron beam properties were evaluated using depth–dose profiles and lateral dose profiles at 10 cm depth in water (Tzedakis *et al.*, 2004). They proposed the use of depth–dose profiles for the determination of initial energy and lateral profiles for adjustment of spot size and mean energy. No dependence on energy spread was found and the angular divergence was ignored.

The tuning of the incident electron beam parameters for two linac models, Elekta Prec*i*se (**Paper II**) and Elekta Synergy (**Paper IV**), were performed in the same iterative way as Tzedakis *et al.* (2004), but also included the angular divergence. Two different models were used in this work based on the development process of a flattening filter-free beam delivered by an Elekta linac. The Elekta Prec*i*se model was among the first accelerator available for measurements at Allgemeines Krankenhaus in Vienna, Austria and at St Luke's Hospital, Dublin, Ireland. A major difference from many previous studies was that a common incident electron beam model was found based on measured data for both flattened and flattening filter-free beams with the same accelerator potential. This was motivated by the fact that the impinging electron beam was not altered between the two modes and the only difference was the presence of a flattening filter or a flat metal disk. Removing the flattening filter was part of the procedure Sawkey and Faddegon (2009) used in their investigation of divergence of the impinging electron beam in a Siemens Oncor linac.

Measured depth–dose profiles for 10×10 cm^2 fields and lateral dose profiles for 20×20 cm^2 fields were used to match the calculated data. The mean energy of the electron beam was varied in steps of 0.1 MeV around the specifications provided by the manufacturer and the energy spread was kept constant at a value specified by the vendor, based on previous findings (Sheikh-Bagheri and Rogers, 2002; Tzedakis *et al.*, 2004). Once the depth–dose profiles for both FF and FFF beams were within 1.5 %, the spot size in both inplane (parallel to the direction of beam acceleration) and crossplane (perpendicular to the direction of beam acceleration) directions as well as the angular deflection of the beam was varied until the lateral dose profiles agreed within 2 % of local dose at -9 cm to +9 cm inside the 20×20 cm^2 fields. If a match was not found the mean energy was varied and both depth–dose and lateral profiles were recalculated.

3 Characteristics of flattening filter-free beams

3.1 Output

As previously mentioned, the two most pronounced effects of removing the flattening filter are the increased output and the forward peaked lateral dose profiles. The relative increase in the dose rate (Gy/min) for a 10×10 cm² field was 1.68, 2.06 and 2.30 for 6 MV untuned (same acceleration potential as FF beam), 6 MV tuned (increased acceleration potential to provide a similar tissue-phantom ratio at 20 cm and 10 cm depth under reference conditions ($TPR_{20,10}$)) and 10 MV untuned, respectively, when a 6 mm Cu plate was used as a replacement filter (**Paper I**). Monte Carlo simulations showed slightly different central axis output ratios of 1.76 for the untuned 6 MV beam and 2.66 for the 10 MV beam (**Paper II**). The difference can be explained by the calibration and hardware limitations of the linac, which affect the delivered dose rates. There are a number of publications reporting increased dose rates of the order of a factor of two higher when the flattening filter is removed (Cashmore, 2008; O'Brien *et al.*, 1991; Vassiliev *et al.*, 2006b).

Conventional linear accelerators with FFF beams available for clinical use are commercially available with dose rates that are 2–4 times higher than the flattened beams (Xiao *et al.*, 2015). The increased dose rate can be advantageous for reducing treatment times. However, other parameters, such as the movement speed of the MLC leaves and, for rotational therapies, the gantry rotation speed, may limit the delivery time reduction for FFF beams.

At the time of publication of **Paper I-III** it was stated that the 6 mm Cu replacement filter was the probable configuration for a future release of a clinical flattening filter-free beam from Elekta. Since the 6 mm Cu filter reduces the output by 18 %–21 % for the two investigated beams a more thorough investigation of the effect of different thicknesses was conducted. One of the major concerns was the signal measured by the internal monitor chamber; thus a study was performed investigating the filter thickness needed for generating the same electron fluence to the monitor chamber as when the flattening filter is present (Lind *et al.*, 2009). It was found that 6 mm Cu is not necessary to provide this but a thinner filter of 3 mm Cu combined with a 2 mm Al

filter back plate would provide the same dose per incident electron to the monitor chamber as when the flattening filter is present (Lind *et al.*, 2009). It was also found that using more than 5 mm Cu did not further reduce the dose to the monitor chamber if the target would fail and the primary electron beam would strike the replacement filter. Additionally, a replacement filter of 3 mm Cu was observed, through Monte Carlo simulations, to provide the same dose to the monitor chamber as a beam with flattening filter and also provide enough filtration to remove scattered radiation from the primary collimator. Following the publication of this study, Elekta modified the design of the replacement filter used in subsequent clinical accelerators, using a 2 mm thick Fe plate instead.

3.2 Depth–dose profiles

The attenuating properties of flattening filter-free photon beams are different from conventional beams due to the difference in beam filtration. If the accelerating potential is kept the same, photon beams with thinner replacement filters discussed previously, will show a steeper dose fall-off at depths beyond the depth of maximum dose since these filters provide less beam hardening than the original flattening filter. Depending on the linac design and settings, the flattening filter-free beams with the same accelerating potential as a conventional 6 MV beam, will generally have a depth–dose distribution corresponding to a 4 MV–5 MV conventional photon beam (Cashmore, 2008; Vassiliev *et al.*, 2006b).

One option, which was investigated, is to increase the acceleration potential of the electrons for the flattening filter-free beam in order to achieve a similar depth–dose deposition as a conventional beam. For the tuned 6 MV beam presented in **Paper I** this was done by increasing the energies of the impinging electrons to provide a beam quality measure, $TPR_{20,10}$, as close to the flattened beam as possible. Figure 3.1 shows Monte Carlo calculated depth–dose profiles for a 10×10 cm^2 field at SSD 100 cm for two beams with a flattening filter and two beams with a replacement filter of 2 mm stainless steel using the Elekta Synergy model from **Paper IV**. The conventional 6 MV flattened beam and the untuned flattening filter-free beam have a mean impinging electron beam energy of 6.3 MeV, while for one of the flattening filter-free beams the impinging electron mean energy has been increased to 8.2 MeV. At this energy the $TPR_{20,10}$ of the flattened and unflattened beams are close to identical (0.684 and 0.683, respectively). Also included is a beam with a flattening filter with a mean energy of the incident electron beam of 5.0 MeV with a $TPR_{20,10}$ of 0.658 which is close to the $TPR_{20,10}$ of 0.657 for the 6 MV FFF untuned beam.
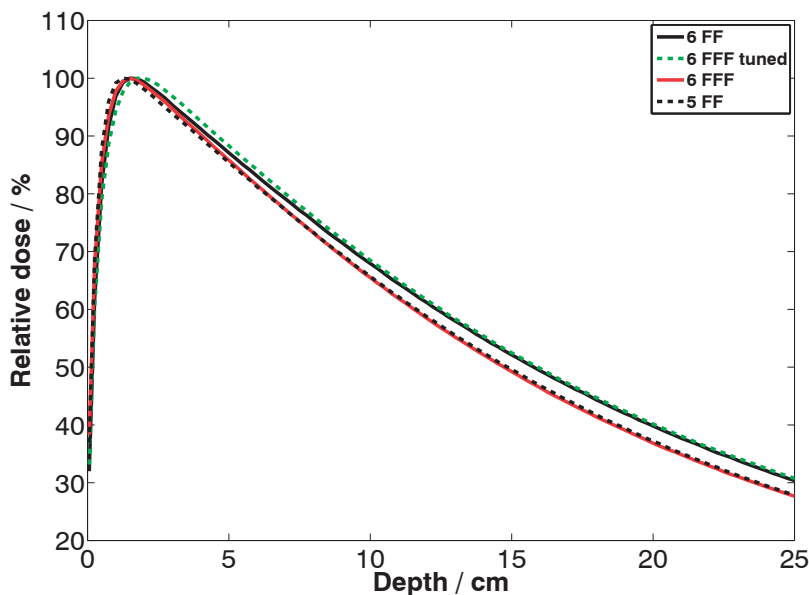
Figure 3.1 Monte Carlo calculated depth dose profiles for beams with and without flattening filter in the beam line with a field size of 10×10 cm² and SSD 100 cm. The solid black line is for a 6 MV beam with flattening filter and the red solid line is for a beam with a 2 mm Fe replacement filter in the beam line (both with a mean energy of the impining electrons of 6.3 MeV). The green dotted line is for a beam with a 2 mm Fe replacement filter for which the mean energy of the impining electron beam has been increased from 6.3 MeV to 8.2 MeV and the black dotted line is for a beam with flattening filter with a mean energy of the impinging electrons of 5 MeV.

The depth of dose maximum (d_{max}) will be affected by the energy reduction and the reduction of scattered radiation when the flattening filter is removed. The two effects counter each other and the differences in d_{max}, with and without a flattening filter, presented in **Paper I** were small. For field sizes between 5×5 cm² and 15×15 cm² the maximal difference between depths of maximum dose for the flattened and unflattened beams was 1 mm. The largest difference found was for the 20×20 cm² field for the 6 MV beams measured in Dublin where the FF beam had a d_{max} that were 3 mm shallower than the FFF beam. In general, the FFF beams had less variation of d_{max} with field size.

Clinical flattening filter-free beams delivered by the Elekta Versa HD are energy matched by setting the relative dose at 10 cm depth for a field size of 10×10 cm² at SSD 100 cm equal to corresponding conventional beams (Paynter *et al.*, 2014; Xiao *et al.*, 2015). Siemens had their flattening filter-free beams, delivered by an Artiste linac, tuned to the depth–dose profile of the conventional beam (Dzierma *et al.*, 2012)

21

whereas Varian has chosen not to alter the accelerating potential for their flattening filter-free beams delivered by the TrueBeam linac (Dzierma *et al.*, 2012; Hrbacek *et al.*, 2011; Xiao *et al.*, 2015). This means that 6 MV FFF beams from Varian and Elekta will have very different attenuating properties since their accelerating potentials differ by about 2 MV while Siemens has chosen to call their energy matched beam 7 UF (Un-Flat).

The dose at the surface of the patient is also affected when the flattening filter is removed. At small field sizes, FFF beams show a larger surface dose while for fields larger than about 15×15 cm^2 the surface dose is smaller for FFF beams. However, surface doses reported in **Paper I** are not corrected for the non-electronic equilibrium in which they are measured. Since measurements were conducted using a plane parallel ion chamber the resulting measurements overestimate the dose in the build-up region (Gerbi and Khan, 1990; Nilsson and Montelius, 1986). Gerbi and Khan (1990) presented a correction factor accounting for the in-scattering of electrons and wall perturbation effects. However, this correction is dependent on the beam quality of the photon beam and the suitability of this method for flattening filter–free photon beams is uncertain. The aim of the study presented in **Paper I** was to compare photon beams delivered with and without a flattening filter and thus to investigate the relative difference in surface dose between the two delivery modes. In Figure 3.2, Monte Carlo calculated surface doses for the untuned 6 MV and 10 MV beams are shown together with the uncorrected measurements of surface doses from **Paper I** for a 10×10 cm^2 field at SSD 100 cm. Compared to MC calculated doses the measurements are overestimating the dose at 1 mm depth by 11 %–14 %. However, the relative difference between the FF and FFF beams are almost the same for the measured and calculated values. The Monte Carlo calculated relative doses for the untuned FFF beams increase the surface dose by 12 % and 17 % for the 6 MV and 10 MV beams, respectively, while the measurements show an increased dose of 13 % and 14 %. For the tuned FFF beam measured in Vienna the relative increase in dose at 1 mm was only 4 % for the same field. The same increase was found through Monte Carlo simulations of a tuned 6 MV FFF beam with a 2 mm Fe replacement filter, which is included in Figure 3.2.

For the same accelerator type, Almberg *et al.* (2012), found an 8 %–10 % increase at 1 mm depth for a tuned 6 MV FFF beam (8.0 MeV initial electron energy) with 2 mm Fe replacement filter and a 20 %–25 % increase for an unturned beam with a 5×5 cm^2 field. Monte Carlo simulations on a Varian True Beam by Javedan *et al.* (2014), showed that the dose at 1 mm depth was increased by about 12 % for an untuned 6 MV beam, with a field size of 25×25 cm^2 and SSD 100 cm.
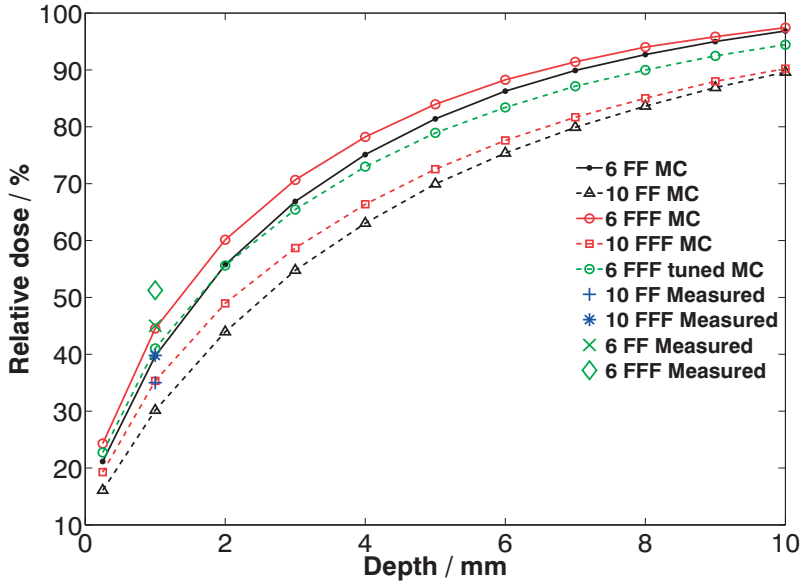
Figure 3.2. Relative surface doses for 6 MV (solid lines) and 10 MV (dotted lines) photon beams with flattening filter (black lines) and with a 6 mm Cu replacement filter (red lines) for a 10×10 cm^2 field at SSD 100 cm. Measured relative surface doses at 1 mm depth for the 6 MV and 10 MV beams are included. The green line is for a tuned 6 MV beam with 2 mm Fe as a replacement filter (8.2 MeV in mean energy of the impinging electrons). The statsitical uncertanty (1 SD) in the calculated data points are within the marker size.

3.3 Spectra

Figure 3.3 shows normalised photon spectra from the four beams used to derive the depth–dose distributions shown in Figure 3.1 (c.f **Paper II** for spectra from Elekta Prec*i*se 6 MV and 10 MV beams with 6 mm copper replacement filter). At the central axis (Figure 3.3a), flattened beams have a larger proportion of higher energy photons than the FFF beams, while at a position close to the field edge of the 40×40 cm^2 field (Figure 3.3b) the spectra are more similar. At the field edge the mean energy of the flattened beams is more than 20 % lower than at the central axis while the mean energy of the FFF beams is about 10 % lower. The smaller variation of beam quality at off-axis positions can be advantageous for some dose calculation algorithms since it reduces the variation in lateral profiles at different depths.
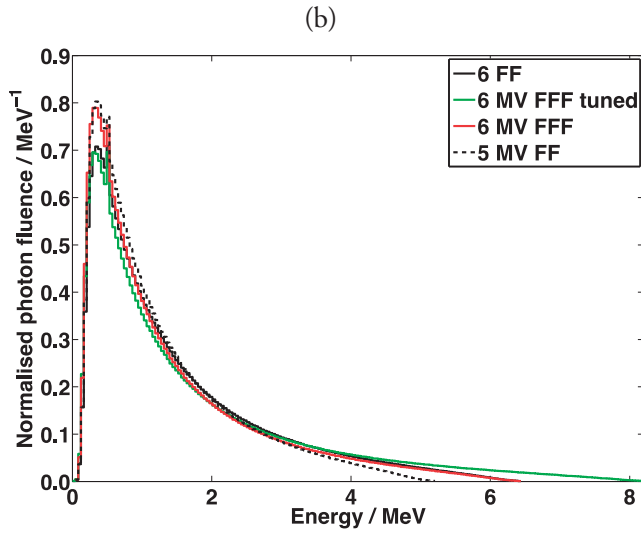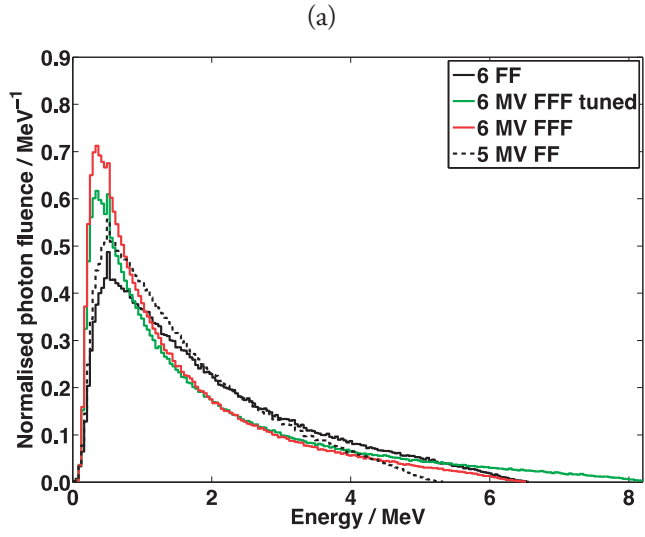
Figure 3.3. Photon fluence spectra in air, normalised per unit total fluence for the four beams described in section 3.2. Data were sampled in a plane normal to the central axis at 100 cm distance from the target for a 40×40 cm² field at the central axis (a) and at the field edge (b).

3.4 Lateral Dose Profiles

When comparing conventional and flattening filter-free beams the most notable differences are the increase in dose rate and the shape of the lateral dose profiles. As mentioned in the previous section FFF lateral dose profiles are much less affected by beam hardening effects at different depths, illustrated by Monte Carlo calculated profiles in Figure 3.4. Here the off-axis distances were set to unity at an off-axis distance where the dose was half of the central axis dose for a 40×40 cm² field at SSD 100 cm and 6 MV. The flattening filter-free beam (Figure 3.4b) has a replacement filter of 2 mm iron and the incident electron energy has been tuned to match $TPR_{20,10}$ of the conventional beam (see **Paper I** for a comparison of a 20×20 cm² field at 10 MV with an untuned FFF beam).
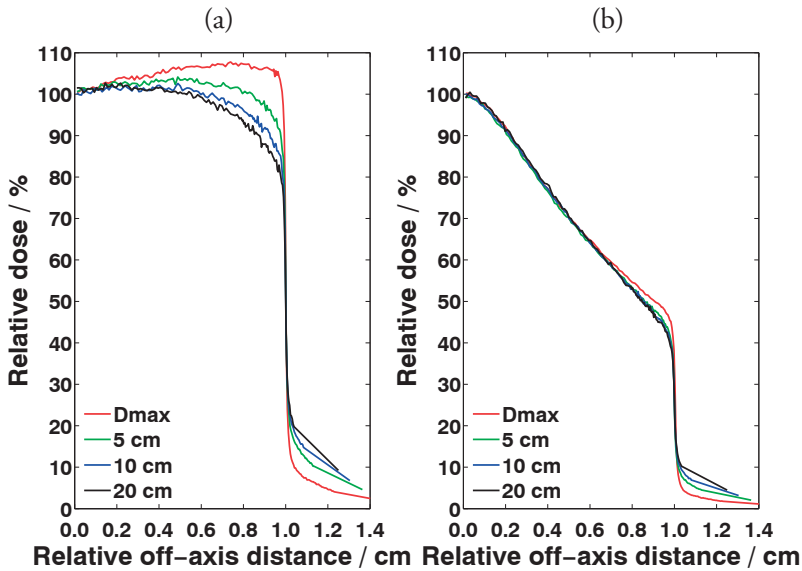
Figure 3.4. Monte Carlo calculated lateral dose profiles at different depths with flattening filter (a) and with a 2 mm Fe replacement filter (b) for a field size of 40×40 cm² at SSD 100 cm. All profiles are normalised to unity at the central axis.

Due to the lateral dose fall-off, FFF profiles have to be re-normalised in order to make the standard definition of penumbral width (distance between the 20 % and 80 % isodose lines) meaningful. In **Paper I**, the lateral dose profiles were rescaled to unity at the inflection point of the curve, as proposed by Ponisch *et al.* (2006), rather than at the central axis. The measured penumbral widths for FFF beams were within 1 mm of the conventional beams, for all field sizes investigated. Cashmore (2008) reported a small reduction of 0.5 mm when the flattening filter was replaced by a 2 mm Al plate on a similar linac model.

3.5 Scatter

Half of all photons originating from other parts of the accelerator head than the target have their last interaction in the flattening filter, before reaching a plane at the isocenter with the field size set to 20×20 cm² (**Paper II**). Figure 3.5 shows the location along the central axis where photons reaching the isocenter plane inside the field edges had their last interaction. The overall reduction in scatter from the treatment head in flattening filter-free mode was calculated to be 31.7 % and 47.6 % for the 6 MV and 10 MV beams, with a calculated statistical uncertainty within 0.03 % (1 SD) (**Paper II**).
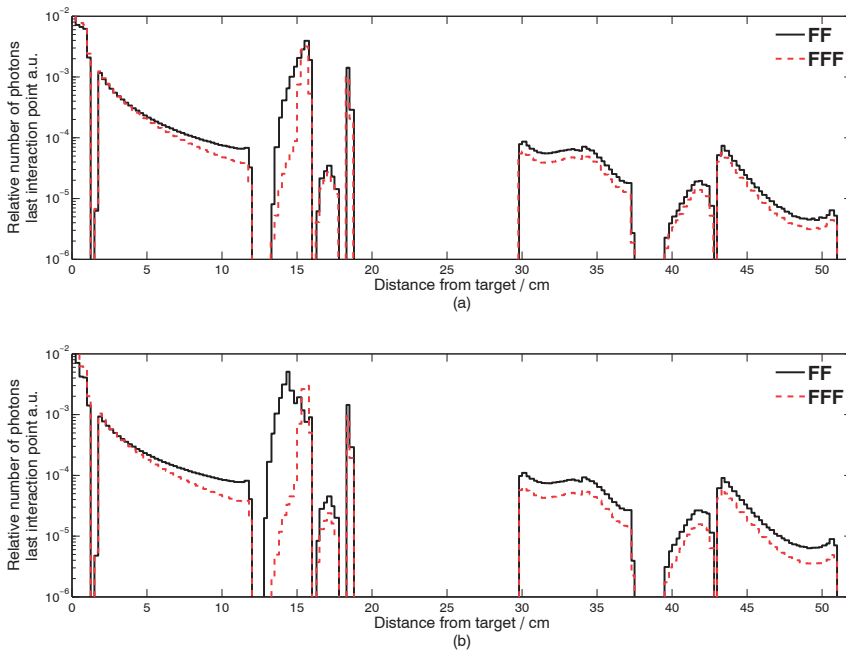
Figure 3.5. Monte Calo calculated relative number of photons for 6 MV (a) and 10 MV (b) last interaction point along the beam axis reaching the isocentre plane at 100 cm from the target, for a field size of 20×20 cm². The solid black lines are for beams with a flattening filter and the dotted red lines are for flattening filter-free beams with a 6 mm Cu replacement filter. The peak to the far left, representing primary, not scattered in the treatment head, photons has been cut for illustrational purposes (Figure from **Paper II**).

This reduction is also seen as the variation of output factor in air (also called head scatter factor or collimator scatter factor) which is smaller for beams with the replacement filter, as shown in Figure 3.6. The head scatter dose has been reported to account for 5 %–15 % of the total dose, depending on beam energy (Ahnesjö, 1994) and this factor is an important parameter for accurate dose calculation in many treatment planning systems (Ahnesjö and Aspradakis, 1999; Fippel *et al.*, 2003; Zhu *et al.*, 2009). The range of readings is significantly decreased when the flattening filter is removed, a variation of the order of 4 % is observed for the 10 MV FFF beam when varying the field size from 3×3 cm^2 to 40×40 cm^2, compared to 9 % variation for the conventional 10 MV beam. For the 6 MV FF beams measured in Vienna and Dublin the head scatter factor varies of the order 8 % while the tuned 6 MV FFF beam in Vienna shows a slightly increased variation of 5 % compared to the untuned beam in Dublin where it was 4.5 %.
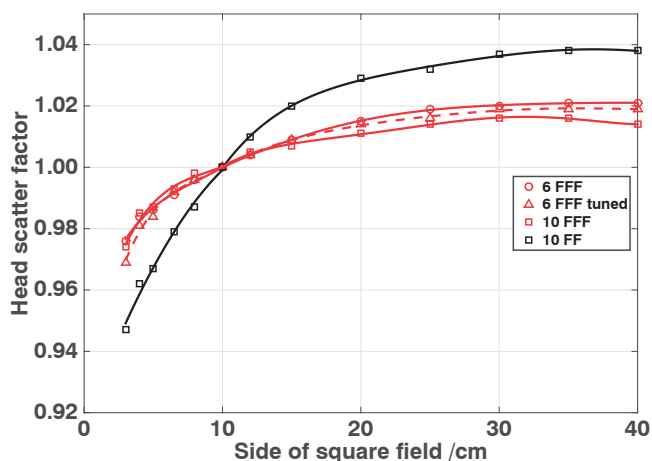
Figure 3.6. Measured head scatter factors for a 10 MV beam with flattening filter and three beams with a 6 mm Cu replacement filter (6 MV and 10 MV) (adapted from **Paper I**).

The beams used in this study show slight deviations from previous findings by Cashmore (2008), who found a reduced variation in head scatter factors for field sizes from 4×4 cm^2 to 40×40 cm^2 from 9 % to 3 % when the flattening filter was replaced by a 2 mm Al replacement filter. For the same field size range corresponding values of 6 % for FF and 2 % for an FFF beam with a 2 mm Fe replacement filter have been reported for an Elekta Agility linac (Richmond *et al.*, 2015). For these field sizes the 6 MV FF beams showed a variation of 6.5 % and the 6 MV FFF beams (both tuned and untuned) varied by 4 % (**Paper I**). However, since the head scatter factor is affected by the design of the accelerator head and in particular the exact material, size and shape

of the flattening or replacement filter, direct comparisons are difficult to make. The overall effect, though, is a reduced variation for beams without a flattening filter.

Through Monte Carlo simulations, the contribution to the head scatter factor from different parts in the accelerator head can be further investigated using the LATCH variable in BEAMnrc,. In Figure 3.7, head scatter factors, calculated as the ratio of primary collision water kerma in free space for any collimator setting to a reference collimator setting ($10{\times}10$ cm^2) for the same number of monitor units MU as defined in Zhu *et al.* (2009) are shown. The primary collision water kerma in free space K_p, was derived from a photon spectra scored in air in a circular region with a radius of 0.5 cm at the central axis 100 cm from the target for a range of collimator settings from $3{\times}3$ cm^2 to $40{\times}40$ cm^2. The calculated head scatter factors were within 0.4 % of measurements performed on a research beam of an Elekta Synergy linac equipped with a 2 mm Fe replacement filter when operating in FFF mode. The variation of head scatter factors for these two beams was in agreement with those reported in a study using the same replacement filter (Richmond *et al.*, 2015).
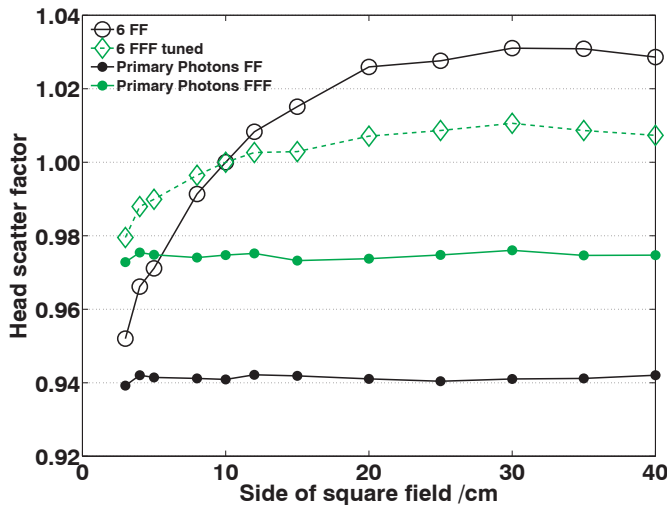

Figure 3.7. Monte Carlo calculated total head scatter factors (open symbols) and the component of the head scatter factor from primary photons (closed symbols) for a flattened beam (black) and an energy tuned photon beam with 2 mm Fe replacement filter. The calculated statistical uncertainty in the total scatter factors are within about 1 % (1 SD).

The contribution to the total head scatter factor from photons interacting in the various components of the accelerator head for a field setting A, can be calculated as:

$$S_c^i(A) = \frac{K_c^i(A)/MU}{K_c^{tot}(A_{ref})/MU} \qquad (3.1)$$

where S_c^i, is the head scatter contribution from photons having interacted in component i, K_c^i and K_c^{tot} are primary collision water kerma for photons having interacted in component i and for all photons, respectively. It should be noted that the same photon can be included in more than one component.

The component from primary photons is, as expected, invariant with field size. The primary photons contribute to 99 %–97 % of the total head scatter factor as the field size is varied from 3×3 cm² to 40×40 cm² for the flattening filter-free photon beam, while this contribution is 98 % to 92 % for the beam with a flattening filter. In Figure 3.8, the contribution from different parts of the accelerator is shown.

For conventional fields, photons having interacted in the flattening filter are the major contributors to the variation in the head scatter factor for fields larger than 10×10 cm², while for smaller fields the contribution from photons interacting in the primary collimator have an equal or even slightly larger impact (Figure 3.8a). However, for the beam with a replacement filter (Figure 3.8b), photons interacting in the primary collimator are the largest contributors to the head scatter factor for all field sizes and the difference in contribution from the filter and secondary collimators are within the uncertainty of the calculated values. The contribution from the replacement filter is lower for the 20×20 cm² field in these calculations than in the results presented in **Paper II**. This is explained by the differences in the replacement filters used (2 mm Fe in Figure 3.8 versus 6 mm Cu in **Paper II**) beam energy (8.2 MeV versus 6.6 MeV), different methods of scoring the scattered radiation and that for the results presented in **Paper II**, photons across the entire field of 20×20 cm² were analysed.

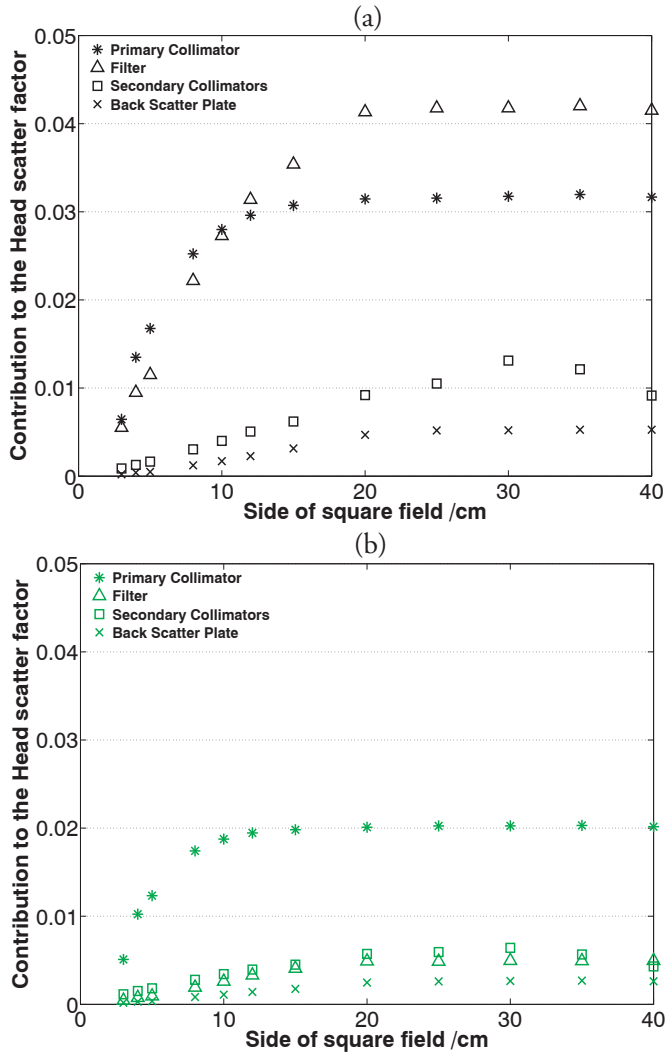**Figure 3.8.** Contribution to the total scatter factor from different accelerator components for a beam with flattening filter (a) and with a 2 mm Fe replacement filter (b). The uncertanty in the calculations are within about 5 % (1 SD).

Phantom scatter factors describe the effects from photons scattered in the phantom volume and they can be derived from the head scatter factor and total scatter factor measurements (Zhu *et al.*, 2009). Due to the lateral dose fall off in FFF beams the scatter contribution to a measurement point located on the central axis will be decreased and thus the phantom scatter factors will be smaller for larger field sizes. As a consequence, comparisons with reference data for phantom scatter factors (NCS, 1998) presented in **Paper I**, showed differences of up to 4 % for the largest field sizes.

3.6 Leakage

Due to the reduced amount of material present in the FFF beam the amount of radiation leakage from the treatment head is expected to be reduced. Leakage measurements in accordance with specifications in the Elekta customer acceptance test were performed (**Paper I**). These showed an average reduction of 52 % for 6 MV beams and 65 % for 10 MV beams with a 6 mm Cu replacement filter compared to beams with a conventional flattening filter.

The MLC is expected to attenuate more radiation in FFF mode since the photon spectra for these beams are softer. Figure 3.9 shows leaf transmission for the 6 MV tuned beam measured in Vienna acquired with radiochromic films (GafChromic EBT, International Speciality Products). The figure shows a larger difference between the two beams at the central axis. As described in **Paper II**, the mean energy of the photons at the central axis are reduced by 0.3 MeV for an untuned beam with a replacement filter thus a reduction of the transmission is expected, while the mean energies at the field edge of a 40×40 cm^2 field are similar for beams with and without a flattening filter and the transmission is therefor similar.
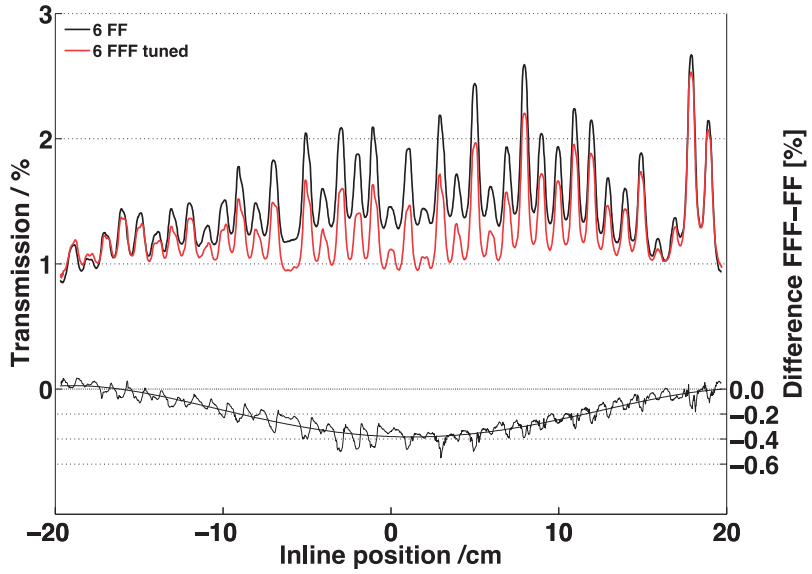
Figure 3.9. Measured leaf transmission for 6 MV beams with a flattening filter (black) and with a 6 mm Cu replacement filter (red). The 6 MV FFF beam has been tuned to the same $TPR_{20,10}$ as the FF beam. The difference in transmission between the two beams was fitted by a polynomial (Figure from **Paper I**).

4 Effect on prediction of stopping power ratios

4.1 Dosimetry

The aim of clinical radiation dosimetry is the precise statement of the absorbed dose at all points of interest in an irradiated patient (ICRU, 1973). The fulfilment of this aim involves several steps:

- Calibration of dosimetry equipment at a Standard Laboratory.

- Determination of absorbed dose at a reference point in water under reference conditions.

- Relative dose distribution in water under non-reference conditions.

- Absorbed dose to the patient under treatment conditions.

This work addresses the second (**Paper III** and **IV**) and third point in this dosimetry chain (**Paper I** and **II**). The first point is based on ionisation chamber dosimetry, water or graphite calorimetry or chemical dosimetry (Fricke) and second point is generally based on ionisation chamber dosimetry while the last two items can be based on other dosimetric methods, e.g. solid-state dosimetry (diodes), thermo–luminescent dosimetry (TLD) and film dosimetry. In clinical practice, however, the final determination of absorbed dose to the patient under treatment conditions is generally performed via calculations in a treatment planning system.

In the following section issues regarding the second point is addressed.

4.1.1 Ionisation Chamber Dosimetry

Ionisation chambers are the most widely used detector for measurement and calibration of the output of clinical radiation therapy treatment machines. The chamber generally consists of an air volume in which an electrical potential is applied. When positioned in a phantom irradiated with indirect ionizing radiation, the release of high-energy electrons in the chamber wall or surrounding media will cause some of these electrons to enter the sensitive volume of the chamber. This leads to ionisation of the air molecules in the cavity and production of positive and negative ions. The charged particles are collected in the electrodes producing the electrical field. The collected charge Q_{ion} is related to the absorbed dose in the air cavity D_{air} with

$$\bar{D}_{air=} \frac{Q_{ion}}{m_{air}} \left(\frac{W}{e}\right)_{air} \tag{4.1}$$

where m_{air} is the mass of the sensitive volume and $(W/e)_{air}$ is the average energy required to produce an ion pair in air per unit charge.

Since the aim is to acquire the absorbed dose to a point in the undisturbed medium (generally water) the dose to the air cavity needs to be converted to dose to medium. This conversion is based on Bragg-Gray or Spencer-Attix cavity theories.

4.1.2 Cavity Theory

The absorbed dose in medium D_{med} is related to the charged particle fluence spectrum $\phi_{med}(E)$ in the medium as:

$$D_{med} = \int_0^{E_{max}} \phi_{med}(E) \left(\frac{S}{\rho}\right)_{med} (E) dE \tag{4.2}$$

where $(S_{col}/\rho)_{med}$ is the unrestricted mass collision stopping power of the medium. Equation (4.2) is only valid if all radiative losses escape the volume of interest and charged particle equilibrium (CPE) exists.

The Bragg-Gray cavity theory relates dose to the cavity to dose to a point in the medium (Attix, 1986). The theory requires the following conditions:

- The cavity is assumed to be small in comparison with the range of the charged particles crossing it such that it negligibly perturbs the charged particle field

- Energy is only deposited from charged particles originating from the surrounding medium

Under these conditions the dose to the medium and air cavity is given by:

$$\frac{D_{\mathrm{med}}}{\overline{D}_{\mathrm{air}}} = \frac{\int_0^{E_{\max}} \phi_{\mathrm{med}}(E)\left(\frac{S_{med}(E)}{\rho}\right) dE}{\int_0^{E_{\max}} \phi_{\mathrm{med}}(E)\left(\frac{S_{air}(E)}{\rho}\right) dE} = \left(\frac{\bar{S}}{\rho}\right)_{\mathrm{med,air}} \tag{4.3}$$

where the unrestricted mass collision stopping power ratio is averaged over the whole spectrum, which according to the first Bragg-Gray condition are the same in the two media.

The use of unrestricted stopping powers requires that no secondary charged particles generated in the cavity escape it. However, charged particles crossing the cavity may generate secondary particles with energies up to $E_{\max}/2$ and some of these electrons would have enough energy to escape the cavity. Spencer and Attix (1955a, 1955b) extended the Bragg-Gray theory to account for the energy deposition of secondary particles generated in the cavity by dividing the electrons into two groups delineated by a cutoff energy Δ.

- Energy losses below Δ are transformed to energy imparted, i.e. they are considered to be locally absorbed.

- For energy losses larger than Δ, no energy is considered locally absorbed and the secondary with energy above Δ is considered as a part of the electron spectrum.

The Spencer-Attix theory was further formulated by Nahum (1978), including a track-end term which represents particles with energies falling below Δ during their passage through the cavity. The Spencer-Attix-Nahum expression is defined as:

$$\frac{D_{\text{med}}}{D_{\text{air}}} = \frac{\int_{\Delta}^{E_{\text{max}}} \phi_{\text{med}}^{\text{SA}}(E) \left(\frac{L_{\Delta,\text{med}}(E)}{\rho}\right) dE + \phi_{\text{med}}^{\text{SA}}(\Delta) \left(\frac{S_{\text{med}}(\Delta)}{\rho}\right) \Delta}{\int_{\Delta}^{E_{\text{max}}} \phi_{\text{med}}^{\text{SA}}(E) \left(\frac{L_{\Delta,\text{air}}(E)}{\rho}\right) dE + \phi_{\text{med}}^{\text{SA}}(\Delta) \left(\frac{S_{\text{air}}(\Delta)}{\rho}\right) \Delta} = s_{\text{med,air}} \quad (4.4)$$

where $\frac{L_{\Delta}(E)}{\rho}$ is the restricted mass collision stopping power at energy E, restricted to energy losses below the cut-off energy, Δ. The electron fluence, $\phi_{\text{med}}^{\text{SA}}(E)$, is the differential electron fluence including secondary electrons and $s_{\text{med,air}}$ is Spencer-Attix mass collision stopping-power ratio averaged over the entire spectrum[4]. The end term in the denominator and numerator are the track-end terms representing energy deposition from electrons falling below the cut-off energy.

The choice of the energy Δ is assumed to represent the cut-off energy at which electrons have enough kinetic energy to pass through the cavity. However, in practice the choice of Δ is more or less arbitrary. In current dosimetry protocols Δ=10 keV is often used as it represents the limit of the Spencer-Attix theory for ionisation chambers in practical use (Andreo, 1994).

The calculations of Spencer-Attix mass collisional stopping power ratios presented in **Paper III** and **IV** were performed using the EGSnrc Monte Carlo code presented in Section 2.4.

The use of Spencer-Attix cavity theory for calculations of dose to the surrounding media still depends on the Bragg-Gray conditions stated above. The deviations from such an idealised ion-chamber are handled with various perturbation factors, correcting the acquired values for the presence of a non-ideal cavity, i.e. a real ion chamber.

4.1.3 Current Dosimetry Protocols for High Energy Photon Beams

Current dosimetry protocols (Codes of Practice) for reference dosimetry (Almond *et al.*, 1999; Andreo *et al.*, 2000) provide procedures for determination of absorbed dose to water in clinical photon beams using calibrated ion chambers. Normally, ion-chambers are calibrated at primary or secondary standard laboratories providing an ion-chamber specific calibration factor $N_{D,w,Q_{Co60}}$. Measurements performed under

---

[4] The notation of $s_{\text{w,air}}$ without a bar is choosen in order to follow the notation in TRS-398.

reference conditions stated by the dosimetry protocol in use can then be used to acquire the absorbed dose to water at the point of measurement in a clinical beam with beam quality Q by

$$D_{w,Q} = M_Q N_{D,w,Q_{Co60}} k_{Q,Q_{Co60}} \qquad (4.5)$$

where M_Q is the influence factor corrected reading of the charge collected by the dosimeter and $k_{Q,Q_{Co60}}$ is a beam quality correction factor correcting the reading for differences between the user beam quality Q and the reference beam quality, in this case 60-Co, Q_{Co60}. The general expression for this factor is (Andreo, 1992)

$$k_{Q,Q_{Co60}} = \frac{(s_{w,air})_Q}{(s_{w,air})_{Q_{Co60}}} \frac{(W_{air})_Q}{(W_{air})_{Q_{Co60}}} \frac{p_Q}{p_{Q_{Co60}}} \approx \frac{(s_{w,air})_Q}{(s_{w,air})_{Q_{Co60}}} \frac{p_Q}{p_{Q_{Co60}}} \qquad (4.6)$$

where W_{air} is the mean energy expended in air per ion pair formed and p represents perturbation factors including departures from an ideal Bragg-Gray cavity. Perturbation factors will not be further dealt with in this thesis. However, in an addendum to the AAPM's TG-51 protocol it is reported that $k_{Q,Q_{Co60}}$ for small ionisation chambers with high-Z electrodes (Z<13) could vary by more than 1 % compared to a beam with flattening filter at the same beam quality, due to the central electrode (McEwen *et al.*, 2014). It should also be noted that influence quantities, especially the ion recombination correction can be affected by the increased dose rate (Kry *et al.*, 2012).

4.1.3.1 Beam Quality Specification for photon beams

The selection of an appropriate beam quality correction factor requires a method of specifying the quality of the photon beam. This parameter can then be used to select the appropriate beam quality conversion and correction factors for the ionisation chamber in use. This section will give an overview of specifiers used in current dosimetry protocols for high-energy photon beams, i.e. IAEA TRS-398 and AAPM TG-51. For a more extensive review of beam quality measures, see e.g. Andreo *et al.* (2000) and ICRU (2001).

The most fundamental beam quality specifier is the complete primary photon spectrum; however, since this is not a feasible approach in clinical high-energy photon beams, more practical approaches have been developed.

The North American dosimetry protocol, i.e. the AAPM's TG-51, defines a beam quality specifier based on the percentage depth–dose at 10 cm depth $\%dd(10)$. However, since contaminating electrons is a problem for normalization at d_{max}, the beam quality is specified as the percentage depth–dose at 10 cm depth in water due to the photon component only $\%dd(10)_x$. According to the protocol, $\%dd(10)=\%dd(10)_x$ for beams below 10 MV. For higher energies the depth–dose distribution is measured by inserting a thin lead foil in the beam line to achieve a state of "known" electron contamination. Then, depending on energy and clearance between the jaws and the phantom surface, one of three relationships between $\%dd(10)$ with the lead foil and $\%dd(10)_x$ is to be selected to end up with the final beam quality specification (Almond *et al.*, 1999).

Another approach has been made in the dosimetry protocol of the IAEA where the tissue–phantom ratio $TPR_{20,10}$ is used as beam quality specifier. $TPR_{20,10}$ is defined as the ratio of absorbed dose to water at depths of 20 cm and 10 cm measured with a constant source-detector distance. The specifier $TPR_{20,10}$ is a measure of the effective attenuation coefficient in a photon beam. There are, however, some uncertainties associated with the use of $TPR_{20,10}$ in photon beams where beams with different filtration can have the same $TPR_{20,10}$ (or the same mean attenuation coefficient) while the $s_{w,air}$ differs by close to 1 % (Brahme and Andreo, 1986; Kosunen and Rogers, 1993). It is stated in the IAEA protocol that the uncertainty in assigning $s_{w,air}$ values to a user beam quality is estimated to be 0.2 %.

4.2 Beam Quality Specification for flattening filter-free photon beams

When the flattening filter is removed the output spectral composition will be altered, affecting the ability to predict stopping power ratios using current beam quality measures. The lateral fluence fall-off will also influence the measurement of TPR and depth–dose. Although the effect on beams with different filtration and the relationship between $TPR_{20,10}$ and $s_{w,air}$ has been known since the mid 1980's (Brahme and Andreo, 1986), Xiong and Rogers (2008) were the first to investigate how the relationship was affected for flattening filter-free beams delivered by clinical linacs. In their study, both $TPR_{20,10}$ and $\%dd(10)_x$ were investigated as beam quality specifiers for conventional photon beams and flattening filter-free beams without a replacement filter in the beam line. They also concluded that $\%dd(10)_x$ was also suitable for the prediction of $s_{w,air}$ (and for k_Q-factors) for flattening filter-free beams, whereas if $TPR_{20,10}$ is used, the resulting k_Q-factors should be lowered by 0.5 % due to the inability of $TPR_{20,10}$ to distinguish between photon beams with a different amount of filtration (Xiong and Rogers, 2008). For treatment units operating without a flattening filter where reference conditions

(e.g. field size and SSD) stated in current code of practices cannot be achieved, methods involving the determination of $\text{TPR}_{20,10}$ for a 10×10 cm^2 field using measurements for an arbitrary field size have been developed (Palmans, 2012; Sauer, 2009). The suggested method in these studies involves the use of a field size "correction" for the reduction in lateral scatter for flattening filter-free photon beams while no correction is made due to differences in filtration of the beams.

A beam quality measure based on the first two moments of the spectral distribution was evaluated for flattening filter–free photon beams using the same photon beams as those used in the study by Xiong and Rogers (2008) (**Paper III**). This beam quality specifier was first introduced by Johnsson *et al.* (2000), who showed that a measure, which qualitatively can be described in terms of the mean ($\bar{\mu}$) and coefficient of variation (c_v) of the relative primary kerma with respect to the linear attenuation coefficient in water, could predict $s_{w,air}$ values for photon beams with different amounts of filtration. These parameters can be derived from narrow-beam transmission measurements at two different depths using a mini-phantom, provided that certain conditions are fulfilled to make the measurement in-air equivalent (Johnsson *et al.*, 1999). However, only a theoretical evaluation of the potential use of this dual-parameter beam quality specifier for flattening filter-free photon beams was addressed in **Paper III**.

In the study by Johnsson *et al.* (2000) the Spencer-Attix mass collision stopping-power ratio $s_{w,air}$, was related to $\bar{\mu}$ and c_v according to

$$s_{w,air} = b_1 + b_2\bar{\mu} - b_3\bar{\mu}^2 + b_4\bar{\mu}^3 - b_5c_v \qquad (4.7)$$

The coefficients b_1-b_5 were re-evaluated using data for beams with and without a flattening filter. The data for the analysis were based on Monte Carlo calculated spectra and $s_{w,air}$ values for nine different beams from 4 MV to 25 MV, with and without a flattening filter (Table I in **Paper III**). The energy spectra used in the calculations were averaged over the entire 10×10 cm^2 field, which leads to slightly softer spectra for the beams with a flattening due to the averaging effect of the spectra over the entire field. However, the spectra used are taken to be representative for "in-air" measurements with a mini-phantom. In Figure 4.1, Monte Carlo calculated $s_{w,air}$ as a function of the spectral mean ($\bar{\mu}$), are shown together with predicted values using Equation (4.7), with the re-evaluated coefficients from **Paper III**. In the figure, data for a TomoTherapy machine and a CyberKnife unit are also included to test the applicability of Equation (4.7) on these flattening filter-free beams. Data for these beams were taken from publications made by Thomas *et al.* (2005) and Araki (2006), respectively. Since the predicted values depends on both $\bar{\mu}$ and c_v, the results based on Equation (4.7) in Figure 4.1 is a 2D projection of a 3D graph (see Figure 2 in **Paper III**).
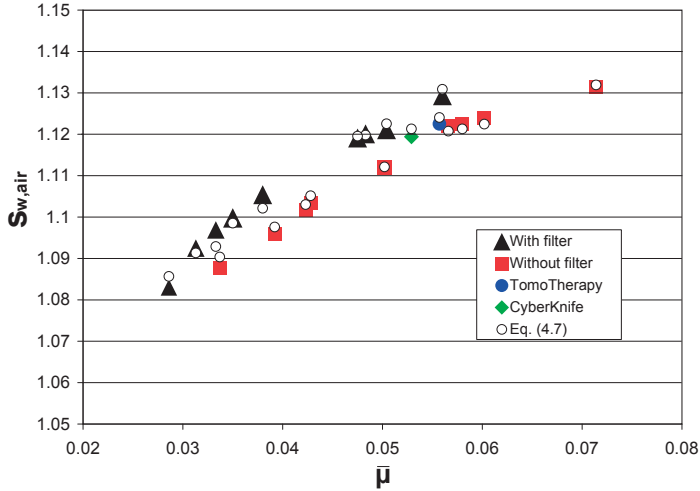
Figure 4.1. Monte Carlo calculated (from Xiong and Rogers (2008), Table I) and predicted (using Eq. (4.7)) stopping-power ratios as a function of the spectral mean for nine different photon beams, with and without flattening filter. One TomoTherapy beam and one CyberKnife beam have also been included (Figure from **Paper III**).

The average of the differences between the predicted and calculated stopping-power ratios for all beams included was 0.02 % ±0.17 % (1 SD). For all beams with a flattening filter the root mean square deviation (RMSD) was 0.2 % and for beams without a flattening filter the root mean square deviation was 0.13 %. The results presented in **Paper III** shows that a beam quality measure which includes both the mean and the coefficient of variation of the linear attenuation coefficient has the potential to predict stopping-power ratios for beams without a flattening filter as well as in conventional beams.

In the study by Xiong and Rogers (2008) it was stated that using $TPR_{20,10}$ as a beam quality measure for flattening filter-free photon beams, the relationship between $TPR_{20,10}$ and stopping-power ratios changes by 0.4 %–1 %. However, in their study, no replacement filter was used in the investigated flattening filter-free beams. Realistic clinical flattening filter-free beams as well as beams with a flattening filter, were used in Monte Carlo calculations of $s_{w,air}$, $TPR_{20,10}$ and $\%dd(10)_x$ described in **Paper IV**. The relationship between the two beam quality measures and $s_{w,air}$ were investigated for photon beams in the energy range 6 MV to 10 MV. It was also investigated if a simple extra parameter, $TPR_{10,5}$, could provide additional information about the properties of the beam and, in combination with $TPR_{20,10}$, be used to increase the accuracy of assigning $s_{w,air}$ to beams without a flattening filter in the beam line. The rationale for this assumption is based on the difference in TPRs at different depths for beams with and without a flattening filter. As shown in Figure 4.2, the difference between the two beams is most pronounced at shallow depths (approximately 2 cm to 6 cm). This

difference is caused by the relative increase of low energy photons in the FFF beams and the difference in lateral dose fall off between the two beams.
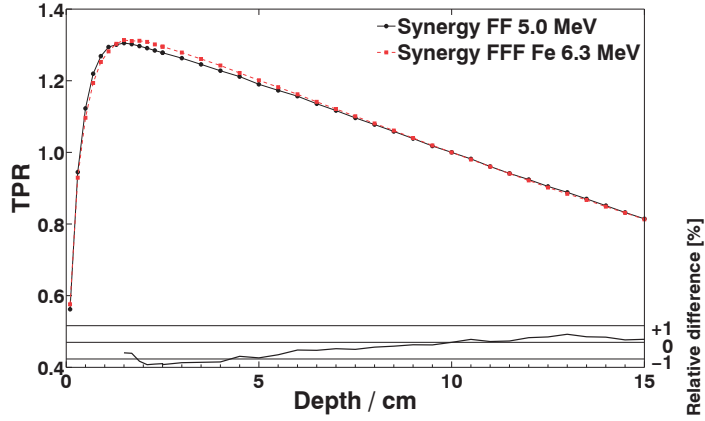

Figure 4.2. Tissue-phantom ratios with different depths for a field size of 10×10 cm^2 and a constant source-surface distance of 100 cm, for one beam with flattening filter and one with a 2 mm Fe replacement filter with similar TPR$_{20,10}$. The TPR values are normalized to unity at 10 cm depth. The calculated statistical uncertainty in each point is estimated to be within 0.15 % (adapted from **Paper IV**).

In the study, 24 photon beams from three medical linear accelerator models were used in the Monte Carlo simulations (Table I in **Paper IV**). One with the complete treatment head of an Elekta Synergy modelled in BEAMnrc, based on specifications by the vendor; one Elekta Prec*i*se and one Varian TrueBeam, for which phase space files generated just above the secondary collimators were acquired. The phase space files for the Elekta Prec*i*se model from (McEwen *et al.*, 2008; Tonkopi *et al.*, 2005) were downloaded from the public IAEA phase space database, while the Varian TrueBeam phase space files (Constantin *et al.*, 2011) were acquired from the vendor. For the Elekta Synergy model the energy of the impinging electron beam was varied so that both the FF and FFF beams covered approximately the same TPR$_{20,10}$ interval (Table I in **Paper IV**). The calculated $s_{w,air}$ were compared to predicted values using the following relationships between $s_{w,air}$ and TPR$_{20,10}$, $\%dd(10)_x$ and the dual beam quality specifier consisting of both TPR$_{20,10}$ and TPR$_{10,5}$

$$s_{w,air} = 1.36138 - 1.9639(\text{TPR}_{20,10}) + 2.53021(\text{TPR}_{20,10})^2 - 1.68964(\text{TPR}_{20,10})^3 \qquad (4.8)$$

$$s_{w,air} = 1.275 - 0.00231(\%dd(10)_x) \qquad (4.9)$$

$$s_{w,air} = 1.258 - 0.00209(\%dd(10)_x) \qquad (4.10)$$

$$s_{w,air} = a_1 + a_2(\text{TPR}_{20,10}) + a_3(\text{TPR}_{10,5}) \qquad (4.11)$$

Equation (4.8) is taken from Andreo (1994) (also in Fig. 23 of Andreo *et al.* (2000)) and is used to investigate the effect on $TPR_{20,10}$ as a beam quality measure for flattening filter-free photon beams. Equation (4.9) is from Rogers and Yang (1999) (referenced in AAPM TG-51 report (Almond *et al.*, 1999)), and was included for evaluation of $\%dd(10)_x$ for flattening filter-free beams. In the study by Xiong and Rogers (2008) Equation (4.10) was presented as a slightly more accurate description of the relationship between $\%dd(10)_x$ and $s_{w,air}$ when flattening filter-free photon beams were used (Equation (2) in Xiong and Rogers (2008)). Finally, a simple bilinear equation including both $TPR_{20,10}$ and $TPR_{10,5}$ was investigated (Equation 4.11). The coefficients a_1–a_3 were determined by least-square fitting of the Monte Carlo calculated data and are given in **Paper IV** (page 3).

In Figure 4.3, $s_{w,air}$ as a function of $TPR_{20,10}$ is shown for the investigated beams. The solid line represents Equation (4.8), and flattening filter-free beams fall below this with an average difference of 0.3 %. This deviation is smaller than the 0.4 % to 1 % reported by Xiong and Rogers (2008), but still lies outside the relative standard uncertainty of 0.2 % in assigning $s_{w,air}$ to beam quality, reported in TRS-398 (Andreo *et al.*, 2000). Open circles are the results based on Equation (4.11), which more accurately predict the $s_{w,air}$ for beams without a flattening filter.

In Table 4.1, the resulting deviations from Monte Carlo calculated $s_{w,air}$ values using equations (4.8)–(4.11) are shown. The maximum deviations using relationships from current dosimetry protocols using either $TPR_{20,10}$ or $\%dd(10)_x$ is about 0.4 %, reported by Xiong and Rogers (2008) as the minimal deviation when using $TPR_{20,10}$ and maximal deviation when using $\%dd(10)_x$. However, as previously reported $\%dd(10)_x$ is more accurate in predicting $s_{w,air}$ in flattening filter-free photon beams. The revised version of equation 4.9, proposed by Xiong and Rogers, reduces the accuracy in predicting $s_{w,air}$ values for the conventional beams with a flattening filter presented in **Paper IV**, indicating that separate relationships between $\%dd(10)_x$ and stopping-power ratios would improve the predictions.

Table 4.1
Summary of deviations in the predicted $s_{w,air}$ values from Monte Carlo calculated for the different beam quality metrics and relationships used in **Paper IV**.

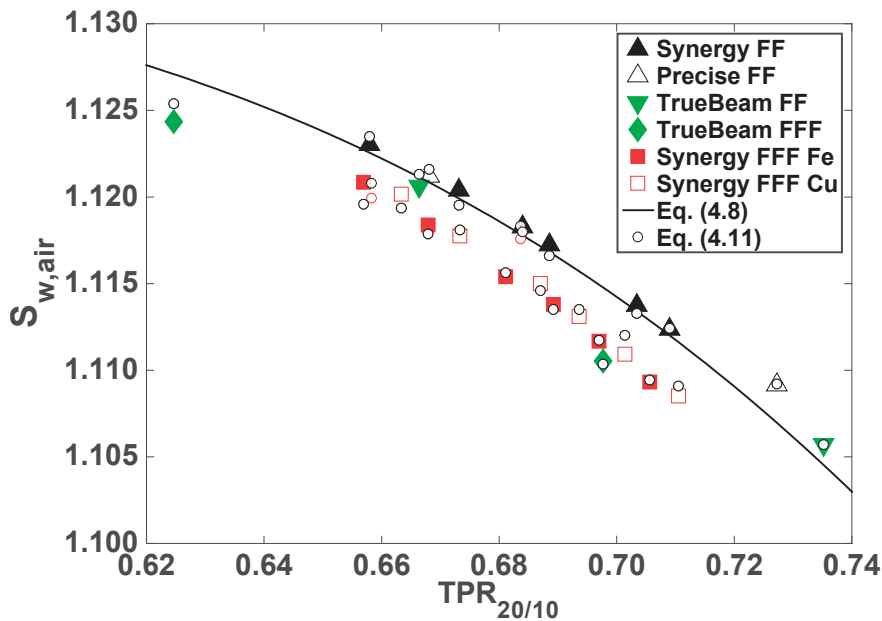|		FFF beams n=14	FF beams n=10	All beams n=24	
Model		RMSD	RMSD	RMSD	Maximum deviation
$TPR_{20,10}$	(Eq. 4.8)	0.0028	0.0009	0.0023	0.39 %
$\%dd(10)_x$	(Eq. 4.9)	0.0017	0.0011	0.0015	0.43 %
$\%dd(10)_x$-revised	(Eq. 4.10)	0.0008	0.0026	0.0018	0.27 %
$TPR_{20,10}$ and $TPR_{10,5}$	(Eq. 4.11)	0.0006	0.0005	0.0006	0.11 %

Figure 4.3. Monte Carlo calculated stopping-power ratios as a function of $TPR_{20,10}$ for all 24 beams used in **Paper IV**. Predicted values using both $TPR_{20,10}$ and $TPR_{10,5}$ (Equation (4.11)) are shown in circles and the solid line is representing Equation 4.8 (in a 3D representation with an additional axis for $TPR_{10,5}$ these data would appear on a plane surface) (Figure from **Paper IV**).

In Figure 4.4, predicted $s_{w,air}$ values using equations (4.8)–(4.11) versus Monte carlo calculated values are shown. Figure 4.4a includes the results for the TPR-based beam quality metrics ($TPR_{20,10}$ and $TPR_{20,10}$ together with $TPR_{10,5}$), while Figure 4.4b includes results based on $\%dd(10)_x$. For the beams investigated, only covering the energy range relevant to the majority of clinical flattening filter-free beams, the use of a dual beam quality metric using two tissue–phantom ratios is more accurate than only using $TPR_{20,10}$.

One could argue that a separate relationship between $s_{w,air}$ and e.g. $TPR_{20,10}$ and $\%dd(10)_x$, could be used for flattening filter-free photon beams. However, this would require a more thorough investigation of the impact of different replacement filters on this relationship. The results presented in **Paper IV**, indicate that using 2 mm Fe or 6 mm Cu in the beam line does not have a large effect on the relationship using either $TPR_{20,10}$ or $\%dd(10)_x$ for an Elekta Synergy, but other combinations of targets and replacement filters might be used in the future.
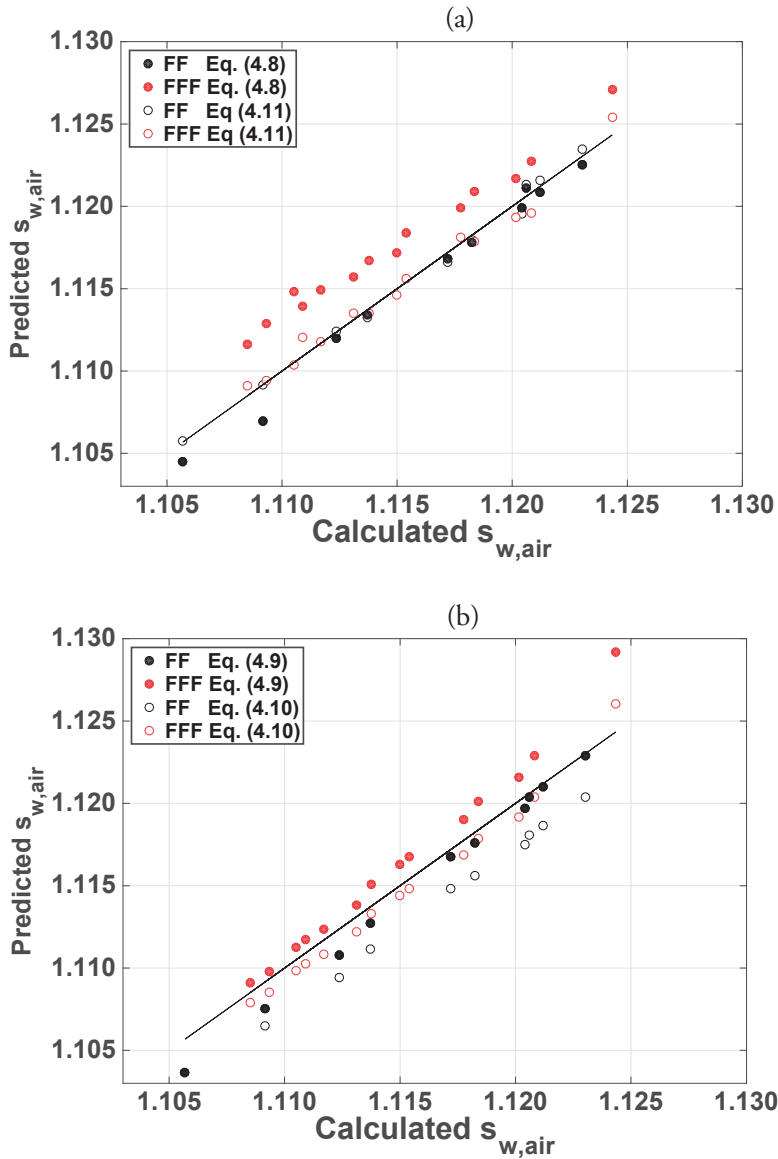
Figure 4.4. Predicted versus Monte Carlo calculated stopping-power values for beams with flattening filter (black circles) and for beams without flattening filter (red circles) using TPR-based quality metrics (a) and based on $\%dd(10)_x$ (b). Predicted values derived from relationships given in two dosimetry protocols (full circles) (Equations (4.8) in (a) and (4.9 in (b)) and for two suggested improved relationships (open circles) (Equation (4.11) in (a) and equation (4.10) in (b)), are shown together with the solid line representing the situation where the predicted values equal calculated values.

5 Conclusions

Both measurements and Monte Carlo simulations of C-arm medical linear accelerators have been performed, operating with and without a flattening filter in the beam line. The effects of removing the flattening filter on the resulting photon beam properties have been investigated. For an Elekta Prec*i*se linac, it was found that the delivered dose per unit time was increased approximately twofold when the flattening filter is removed (**Paper I and II**). This increase reflects a reduction of photons absorbed or scattered in the flattening filter and it was found that the scatter from the treatment head was reduced by 30 %–45 %. The variation of scattered radiation with field size is also reduced (**Paper II**). These findings indicate that the dose outside the treatment fields can be reduced. The photon energy spectra for flattening filter-free beams are softer (**Paper II**) resulting in steeper absorbed dose fall-off with depth (**Paper I**) and less lateral energy variation across the field (**Paper II**). By increasing the acceleration potential of the linac, the output will increase even further and the depth–dose profiles become more similar to the equivalent conventional photon beam (**Paper I**). The studies described in **Paper I** and **II** were conducted based on a research beam line provided by the manufacturer. Based on findings presented in Lind *et al.* (2009) the clinical release of a photon beam with flattening filter-free capabilities included a modified beam line with a thinner replacement filter.

With the recent increase in clinical flattening filter-free beams used in radiotherapy treatments, questions regarding the use of international ion chamber dosimetry protocols were raised. A previously proposed beam quality specifier was shown to accurately predict stopping-power ratios in both flattened and flattening filter-free photon beams (**Paper III**). Two beam quality-specifiers used in international ion chamber dosimetry protocols were evaluated for flattening filter-free beams and it was found that both could safely be used for these beams without substantially increasing the uncertainty in the absorbed dose delivery to the patient. A new beam-quality measure was introduced and evaluated to improve the prediction of stopping-power ratios in radiotherapy photon beams (**Paper IV**). The relationship between stopping-power ratios and this new beam quality specifier was shown to be a simple bi-linear equation.

Future investigations

Flattening filter-free photon beams are now available from all major manufacturers of clinical medical linear accelerators. Both the CyberKnife and TomoTherapy machines have demonstrated that a flattening filter is not necessary for planning and delivery of advanced treatment techniques such as stereotactic and intensity modulated treatments. With the release of conventional C-arm medical linacs from Elekta, Varian, and Siemens the flattening filter-free treatments are now wide-spread. However, several issues remain to be solved and investigated further. There is no clear set of standardised specifications of some beam parameters such as beam flatness and penumbra for flattening filter-free photon beams, although several suggestions exist in the literature (Fogliata *et al.*, 2012; Ponisch *et al.*, 2006). There is also a need for verification of the results presented in **Paper IV**. This could be achieved by measurement of the k_Q factor through calorimetric or chemical (Fricke) dosimetry. There are initial results indicating no difference in the measured k_Q factor for beams with and without a flattening filter for photon beams where the FFF beam is tuned to the same relative dose at 10 cm depth (De Prez *et al.*, 2015). However, more studies are needed in this area to verify the use of current codes of practice for ion chamber dosimetry in flattening filter-free photon beams. In this work the effect on perturbation factors for flattening filter-free beams have not been investigated. Monte Carlo calculated beam quality correction factors k_Q for beams without a flattening filter could provide further information about the use of FFF beams in current codes of practice. In future work, such simulations need detailed information of a range of real ionisation chambers.

Different linac vendors have chosen different approaches for the energy of the flattening filter-free beams. The effect of these differences has not been properly studied and a thorough investigation of the advantages and disadvantages of the different methods would provide valuable information. Differences in, e.g. dose bath effects and surface doses could be present and needs to be further studied.

FFF beams have been investigated at a large number of treatment sites and found to be advantageous for IMRT treatments, especially for small targets and high fractional doses. However, there is no general consensus as to which modulated treatments that would most benefit from FFF mode.

The increased dose rate could also prove to be an advantage in minimising the effect of target movement through the shorter exposure times needed. Since the main advantage seen is in reduced treatment times, which is often limited by the rotational speed of the C-arm linac (set to a maximum of one minute for one rotation due to safety reasons) (Gasic *et al.*, 2014), mimicking the TomoTherapy unit in encapsulating the C-arm could further decrease the treatment times and the gain in doing so should be investigated.

Acknowledgements

This thesis has in no way been a 'one man show'. I am forever grateful to all of you from whom I have been receiving help and support from during the completion of this work. In particular, I wish to express my sincere gratitude to:

my main scientific supervisor *Tommy Knöös* whose extensive international network led me into the field of flattening filter-free photon beams. Your scientific skills and ability to provide consistently good advice and guidance is the foundation on which this thesis is built upon.

my scientific supervisor *Crister Ceberg* for always having time to answer my questions and your infectious enthusiasm. Your knowledge and sincere wish to help and improve others is admirable. I hope to continue working with you.

my scientific supervisor *Elinore Wieslander* for helping me despite your heavy workload. You are always encouraging and willing to share your knowledge.

Lee Ambolt for he is truly great, particularly in English, board games and odd jokes.

my co-authors in Dublin; *Brendan McClean* and *Patrick McCavana* for your guidance and for giving me the opportunity to do part of this work in Dublin.

my co-authors in Vienna; *Gabriele Kragl*, *Dietmar Georg* and *Barbara Knäusl* for valuable collaboration and support.

Sacha af Wetterstedt for being a valued friend and colleague in Dublin, Malmö and Lund.

Richard Cronholm for your generous Monte Carlo related assistance and friendship.

Kevin Brown and *Magne Johansson* from Elekta oncology systems for your R&D and technical support.

all my current and former colleagues at radiotherapy treatment physics at Skåne University Hospital, Lund. Special thanks are due to *Sven Bäck* and *Andrej Tomaszewicz* for your help in arranging my clinical work to fit around me working on this thesis and to *Per Wendel*, *Börje Blad* and *Anders Olsson* for your engineering support and for keeping the computer cluster happily working for me.

my friends and colleagues at the department of Medical Radiation Physics, Lund University, Lund.

the most important people in my life my *parents*, *brothers* and my own wonderful family. Thank you for always believing in me. Thank you my lovely *Elin Dalaryd* for your never ending support and love. You are always digging me up when I'm down.

my darlings *ELLA* och *JULIA* – NI ÄR FANTASTISKA!

References

Adler J R, Jr., Chang S D, Murphy M J, Doty J, Geis P and Hancock S L 1997 The Cyberknife: a frameless robotic system for radiosurgery *Stereotact Funct Neurosurg* **69** 124-8

Ahnesjö A 1994 Analytic modeling of photon scatter from flattening filters in photon therapy beams *Med Phys* **21** 1227-35

Ahnesjö A and Aspradakis M M 1999 Dose calculations for external photon beams in radiotherapy *Phys Med Biol* **44** R99-155

Almberg S S, Frengen J and Lindmo T 2012 Monte Carlo study of in-field and out-of-field dose distributions from a linear accelerator operating with and without a flattening-filter *Med Phys* **39** 5194-203

Almond P R, Biggs P J, Coursey B M, Hanson W F, Huq M S, Nath R and Rogers D W 1999 AAPM's TG-51 protocol for clinical reference dosimetry of high-energy photon and electron beams *Med Phys* **26** 1847-70

Andreo P 1991 Monte Carlo techniques in medical radiation physics *Phys Med Biol* **36** 861-920

Andreo P 1992 Absorbed dose beam quality factors for the dosimetry of high-energy photon beams *Phys Med Biol* **37** 2189

Andreo P 1994 Improved calculations of stopping-power ratios and their correlation with the quality of therapeutic photon beams *Proc. Int. Symp. on Measurement Assurance in Dosimetry (Vienna, 1993)(IAEA-SM-330/35)(Vienna: IAEA)* 335-59

Andreo P, Burns D T, Hohlfeld K, Huq M S, Kanai T, Laitano F, Smythe V G and Vynckier S 2000 Absorbed dose determination in external beam radiotherapy *International Atomic Energy Agency, Vienna, IAEA Technical Report Series No. 398*

Araki F 2006 Monte Carlo study of a Cyberknife stereotactic radiosurgery system *Med Phys* **33** 2955-63

Attix F H 1986 *Introduction to Radiological Physics and Radiation Dosimetry* (New York: Wiley)

Berger M J 1963 Monte Carlo calculation of the penetration and diffusion of fast charged particles *Methods in Computational Physics,* ed B Alder, S Fernbach and M Rotenberg (New York: Academic) pp 135-215

Bielajew A F 2013 History of Monte Carlo *Monte Carlo Techniques in Radiation Therapy. Imaging in Medical Diagnosis and Therapy,* ed J Seco and F Verhaegen (Boca Raton, FL: CRC Press, Taylor & Francis Group) pp 3-16

Brahme A and Andreo P 1986 Dosimetry and quality specification of high energy photon beams *Acta Radiol Oncol* **25** 213-23

Brahme A, Chavaudra J, Landberg T, McCullough E C, Nüsslin F, Rawlinson J A, Svensson G and Svensson H 1988 Accuracy requirements and quality assurance of external beam therapy with photons and electrons *Acta Oncol* **27** Suppl. 1

Brahme A, Kraepelien T and Svensson H 1980 Electron and photon beams from a 50 MeV racetrack microtron *Acta Radiol Oncol* **19** 305-19

Cashmore J 2008 The characterization of unflattened photon beams from a 6 MV linear accelerator *Phys Med Biol* **53** 1933-46

Cashmore J 2013 Operation, characterisation and physical modelling of unflattened medical linear accelerator beams and their application to radiotherapy treatment planning. *PhD Thesis* School of Physics and Astronomy, University of Birmingham, England

Constantin M, Perl J, LoSasso T, Salop A, Whittum D, Narula A, Svatos M and Keall P J 2011 Modeling the TrueBeam linac using a CAD to Geant4 geometry implementation: Dose and IAEA-compliant phase space calculations *Med Phys* **38** 4018-24

De Prez L A, Jansen B J, De Pooter J A, Perik T J and Wittkämper F W 2015 OC-0552: First direct comparison of measured kQ values for FFF and FF clinical photon beams *Radiotherapy and Oncology* **115, Supplement 1** S268-S9

Ding G X, Rogers D W and Mackie T R 1995 Calculation of stopping-power ratios using realistic clinical electron beams *Med Phys* **22** 489-501

Dzierma Y, Licht N, Nuesken F and Ruebe C 2012 Beam properties and stability of a flattening-filter free 7 MV beam-an overview *Med Phys* **39** 2595-602

Fippel M 2013 Variance Reduction Techniques *Monte Carlo techniques in radiation therapy,* ed J Seco and F Verhaegen 3 (Boca Raton: CRC/Taylor & Francis) pp 29-39

Fippel M, Haryanto F, Dohm O, Nusslin F and Kriesen S 2003 A virtual photon energy fluence model for Monte Carlo dose calculation *Med Phys* **30** 301-11

Fogliata A, Garcia R, Knoos T, Nicolini G, Clivio A, Vanetti E, Khamphan C and Cozzi L 2012 Definition of parameters for quality assurance of flattening filter free (FFF) photon beams in radiation therapy *Med Phys* **39** 6455-64

Fu W, Dai J, Hu Y, Han D and Song Y 2004 Delivery time comparison for intensity-modulated radiation therapy with/without flattening filter: a planning study *Phys Med Biol* **49** 1535-47

Gasic D, Ohlhues L, Brodin N P, Fog L S, Pommer T, Bangsgaard J P and Munck Af Rosenschold P 2014 A treatment planning and delivery comparison of volumetric modulated arc therapy with or without flattening filter for gliomas, brain metastases, prostate, head/neck and early stage lung cancer *Acta Oncol* **53** 1005-11

Gerbi B J and Khan F M 1990 Measurement of dose in the buildup region using fixed-separation plane-parallel ionization chambers *Med Phys* **17** 17-26

Hrbacek J, Lang S and Klock S 2011 Commissioning of photon beams of a flattening filter-free linear accelerator and the accuracy of beam modeling using an anisotropic analytical algorithm *Int J Radiat Oncol Biol Phys* **80** 1228-37

ICRP 2000 *Prevention of Accidental Exposures to Patients Undergoing Radiation Therapy*, ICRP Publication 86, Annals of the ICRP 30, International Commission on Radiological Protection

ICRU 1973 *Measurment of absorbed dose in a phantom irradiated by a single beam of X or gamma rays*, ICRU Report 23 (Washington,DC: International Commission on Radiation Units and Measurements)

ICRU 1976 *Determination of absorbed dose in a patient irradiated by beams of X or gamma rays in radiotherapy procedures*, ICRU Report 24 (Bethesda, MD: International Commission on Radiation Units and Measurements)

ICRU 2001 *Dosimetry of High-Energy Photon Beams based on Standards of Absorbed Dose to Water*, ICRU Report 64 (Bethesda, MD: International Commission on Radiation Units and Measurements)

Izewska J 1993 Shaping of photon beams from electron linear accelerators in radiation therapy *Med Phys* **20** 171-7

Javedan K, Feygelman V, Zhang R R, Moros E G, Correa C R, Trotti A, Li W and Zhang G G 2014 Monte Carlo comparison of superficial dose between flattening filter free and flattened beams *Phys Med* **30** 503-8

Jeraj R, Mackie T R, Balog J, Olivera G, Pearson D, Kapatoes J, Ruchala K and Reckwerdt P 2004 Radiation characteristics of helical tomotherapy *Med Phys* **31** 396-404

Johnsson S A, Ceberg C P, Knoos T and Nilsson P 1999 Transmission measurements in air using the ESTRO mini-phantom *Phys Med Biol* **44** 2445-50

Johnsson S A, Ceberg C P, Knoos T and Nilsson P 2000 On beam quality and stopping power ratios for high-energy x-rays *Phys Med Biol* **45** 2733-45

Karlsson M, Svensson H, Nyström H and Stenberg J 1988 The 50 MeV Racetrack accelerator. A new approach to beam shaping and modulation. *Proc. Symp. on Dosimetry in Radiotherapy (Vienna, 1988)(IAEA-SM-298/68)(Vienna: IAEA) vol. 2* 307-20

Kawrakow I 2000a Accurate condensed history Monte Carlo simulation of electron transport. I. EGSnrc, the new EGS4 version *Med Phys* **27** 485-98

Kawrakow I 2000b Accurate condensed history Monte Carlo simulation of electron transport. II. Application to ion chamber response simulations *Med Phys* **27** 499-513

Kawrakow I, Mainegra-Hing E, Rogers D W O, Tessier F and Walters B R B 2011 The EGSnrc code system: Monte Carlo simulation of electron and photon transport *Technical Report* PIRS-701 (Ottawa, Canada: National Research Council Canada)

Kawrakow I, Rogers D W and Walters B R 2004 Large efficiency improvements in BEAMnrc using directional bremsstrahlung splitting *Med Phys* **31** 2883-98

Kosunen A and Rogers D W 1993 Beam quality specification for photon beam dosimetry *Med Phys* **20** 1181-8

Kry S, Popple R, Molineu A and Followill D 2012 Ion Recombination Correction Factors (Pion) for Varian TrueBeam High Dose Rate Therapy Beams *Med Phys* **39** 3790-

Kry S F, Howell R M, Polf J, Mohan R and Vassiliev O N 2009 Treatment vault shielding for a flattening filter-free medical linear accelerator *Phys Med Biol* **54** 1265-73

Kry S F, Howell R M, Titt U, Salehpour M, Mohan R and Vassiliev O N 2008 Energy spectra, sources, and shielding considerations for neutrons generated by a flattening filter-free Clinac *Med Phys* **35** 1906-11

Kry S F, Titt U, Ponisch F, Vassiliev O N, Salehpour M, Gillin M and Mohan R 2007 Reduced neutron production through use of a flattening-filter-free accelerator *Int J Radiat Oncol Biol Phys* **68** 1260-4

Kry S F, Vassiliev O N and Mohan R 2010 Out-of-field photon dose following removal of the flattening filter from a medical accelerator *Phys Med Biol* **55** 2155-66

Lind M, Knöös T, Ceberg C, Wieslander E, McClean B and Georg D 2009 Photon beam characteristics at monitor chamber level in a flattening filter free linac: a Monte Carlo study *Radiother Oncol* **92, Supplement 1** S57

Mackie T R, Holmes T, Swerdloff S, Reckwerdt P, Deasy J O, Yang J, Paliwal B and Kinsella T 1993 Tomotherapy: a new concept for the delivery of dynamic conformal radiotherapy *Med Phys* **20** 1709-19

McCall R C, McIntyre R D and Turnbull W G 1978 Improvement of linear accelerator depth-dose curves *Med Phys* **5** 518-24

McEwen M, DeWerd L, Ibbott G, Followill D, Rogers D W, Seltzer S and Seuntjens J 2014 Addendum to the AAPM's TG-51 protocol for clinical reference dosimetry of high-energy photon beams *Med Phys* **41** 041501

McEwen M R, Kawrakow I and Ross C K 2008 The effective point of measurement of ionization chambers and the build-up anomaly in MV x-ray beams *Med Phys* **35** 950-8

Mesbahi A 2009 A Monte Carlo study on neutron and electron contamination of an unflattened 18-MV photon beam *Appl Radiat Isot* **67** 55-60

Mesbahi A, Mehnati P, Keshtkar A and Farajollahi A 2007 Dosimetric properties of a flattening filter-free 6-MV photon beam: a Monte Carlo study *Radiat Med* **25** 315-24

Mesbahi A and Nejad F S 2008 Monte Carlo study on a flattening filter-free 18-MV photon beam of a medical linear accelerator *Radiat Med* **26** 331-6

Mijnheer B J, Battermann J J and Wambersie A 1987 What degree of accuracy is required and can be achieved in photon and neutron therapy? *Radiother Oncol* **8** 237-52

Mohan R, Chui C and Lidofsky L 1985 Energy and angular distributions of photons from medical linear accelerators *Med Phys* **12** 592-7

Nahum A E 1978 Water/air mass stopping power ratios for megavoltage photon and electron beams *Phys Med Biol* **23** 24-38

NCS 1998 Determination and use of scatter factors of megavoltage photon beams *Netherlands Commission on Radiation Dosimetry, Delft, NRC Report 12*

Nelson W R, Hirayama H and Rogers D W O 1985 The EGS4 code system *Report,* SLAC-265 (Stanford, CA: Stanford Linear Accelerator Center)

Nilsson B and Montelius A 1986 Fluence perturbation in photon beams under nonequilibrium conditions *Med Phys* **13** 191-5

Nyström H and Thwaites D I 2008 Physics and high-technology advances in radiotherapy: are they still worth it? *Radiother Oncol* **86** 1-3

O'Brien P F, Gillies B A, Schwartz M, Young C and Davey P 1991 Radiosurgery with unflattened 6-MV photon beams *Med Phys* **18** 519-21

Palmans H 2012 Determination of the beam quality index of high-energy photon beams under nonstandard reference conditions *Med Phys* **39** 5513-9

Paynter D, Weston S J, Cosgrove V P, Evans J A and Thwaites D I 2014 Beam characteristics of energy-matched flattening filter free beams *Med Phys* **41** 052103

Petti P L, Goodman M S, Gabriel T A and Mohan R 1983 Investigation of buildup dose from electron contamination of clinical photon beams *Med Phys* **10** 18-24

Ponisch F, Titt U, Vassiliev O N, Kry S F and Mohan R 2006 Properties of unflattened photon beams shaped by a multileaf collimator *Med Phys* **33** 1738-46

Richmond N, Allen V, Daniel J, Dacey R and Walker C 2015 A comparison of phantom scatter from flattened and flattening filter free high-energy photon beams *Med Dosim* **40** 58-63

Rodriguez M, Sempau J, Fogliata A, Cozzi L, Sauerwein W and Brualla L 2015 A geometrical model for the Monte Carlo simulation of the TrueBeam linac *Phys Med Biol* **60** N219-29

Rogers D W 2006 Fifty years of Monte Carlo simulations for medical physics *Phys Med Biol* **51** R287-301

Rogers D W, Faddegon B A, Ding G X, Ma C M, We J and Mackie T R 1995 BEAM: a Monte Carlo code to simulate radiotherapy treatment units *Med Phys* **22** 503-24

Rogers D W O and Bielajew A F 1990 Monte Carlo techniques of electron and photon transport for radiation dosimetry *The Dosimetry of Ionizing Radiation,* ed K R Kase, B E Bjärngard and F H Attix (New York: Academic) pp 427–539

Rogers D W O, Kawrakow I, Seuntjens J P, Walters B R B and Mainegra-Hing E 2011a NRC user codes for EGSnrc *Technical Report* PIRS-702 (rev C) (Ottawa, Canada: National Research Council Canada)

Rogers D W O, Walters B and Kawrakow I 2011b BEAMnrc Users Manual *Technical Report* PIRS-509(A) revL (Ottawa, Canada: National Research Council Canada)

Rogers D W O and Yang C L 1999 Corrected relationship between %dd(10)x and stopping-power ratios *Med Phys* **26** 538-40

Sauer O A 2009 Determination of the quality index (Q) for photon beams at arbitrary field sizes *Med Phys* **36** 4168-72

Sawkey D L and Faddegon B A 2009 Determination of electron energy, spectral width, and beam divergence at the exit window for clinical megavoltage x-ray beams *Med Phys* **36** 698-707

Seco J and Verhaegen F 2013 *Monte Carlo Techniques in Radiation Therapy. Imaging in Medical Diagnosis and Therapy* (Boca Raton, FL: CRC Press, Taylor & Francis Group)

Sheikh-Bagheri D and Rogers D W 2002 Sensitivity of megavoltage photon beam Monte Carlo simulations to electron beam and other parameters *Med Phys* **29** 379-90

Sixel K E and Faddegon B A 1995 Calculation of x-ray spectra for radiosurgical beams *Med Phys* **22** 1657-61

Sixel K E and Podgorsak E B 1994 Buildup region and depth of dose maximum of megavoltage x-ray beams *Med Phys* **21** 411-6

Spencer L V and Attix F H 1955a A cavity ionization theory including the effects of energetic secondary electrons *Radiology* **64** 113

Spencer L V and Attix F H 1955b A theory of cavity ionization *Radiat Res* **3** 239-54

Thomas S D, Mackenzie M, Rogers D W and Fallone B G 2005 A Monte Carlo derived TG-51 equivalent calibration for helical tomotherapy *Med Phys* **32** 1346-53

Titt U, Vassiliev O N, Ponisch F, Dong L, Liu H and Mohan R 2006a A flattening filter free photon treatment concept evaluation with Monte Carlo *Med Phys* **33** 1595-602

Titt U, Vassiliev O N, Ponisch F, Kry S F and Mohan R 2006b Monte Carlo study of backscatter in a flattening filter free clinical accelerator *Med Phys* **33** 3270-3

Tonkopi E, McEwen M R, Walters B R and Kawrakow I 2005 Influence of ion chamber response on in-air profile measurements in megavoltage photon beams *Med Phys* **32** 2918-27

Tzedakis A, Damilakis J E, Mazonakis M, Stratakis J, Varveris H and Gourtsoyiannis N 2004 Influence of initial electron beam parameters on Monte Carlo calculated absorbed dose distributions for radiotherapy photon beams *Med Phys* **31** 907-13

Vassiliev O N, Kry S F, Chang J Y, Balter P A, Titt U and Mohan R 2009 Stereotactic radiotherapy for lung cancer using a flattening filter free Clinac *J Appl Clin Med Phys* **10** 14-21

Vassiliev O N, Kry S F, Kuban D A, Salehpour M, Mohan R and Titt U 2007 Treatment-planning study of prostate cancer intensity-modulated radiotherapy with a Varian Clinac operated without a flattening filter *Int J Radiat Oncol Biol Phys* **68** 1567-71

Vassiliev O N, Titt U, Kry S F, Ponisch F, Gillin M T and Mohan R 2006a Monte Carlo study of photon fields from a flattening filter-free clinical accelerator *Med Phys* **33** 820-7

Vassiliev O N, Titt U, Ponisch F, Kry S F, Mohan R and Gillin M T 2006b Dosimetric properties of photon beams from a flattening filter free clinical accelerator *Phys Med Biol* **51** 1907-17

Verhaegen F and Seuntjens J 2003 Monte Carlo modelling of external radiotherapy photon beams *Phys Med Biol* **48** R107-64

Walters B, Kawrakow I and Rogers D W O 2007 DOSXYZnrc Users Manual *Technical Report* PIRS-794 (Ottawa, Canada: National Research Council Canada)

Walters B R, Kawrakow I and Rogers D W 2002 History by history statistical estimators in the BEAM code system *Med Phys* **29** 2745-52

Xiao Y, Kry S F, Popple R, Yorke E, Papanikolaou N, Stathakis S, Xia P, Huq S, Bayouth J, Galvin J and Yin F-F 2015 Flattening filter-free accelerators: a report from the AAPM Therapy Emerging Technology Assessment Work Group *J Appl Clin Med Phys* **16** 12-29

Xiong G and Rogers D W O 2008 Relationship between %dd(10)x and stopping-power ratios for flattening filter free accelerators: A Monte Carlo study *Med Phys* **35** 2104-9

Zanini A, Durisi E, Fasolo F, Ongaro C, Visca L, Nastasi U, Burn K W, Scielzo G, Adler J O, Annand J R and Rosner G 2004 Monte Carlo simulation of the photoneutron field in linac radiotherapy treatments with different collimation systems *Phys Med Biol* **49** 571-82

Zefkili S, Kappas C and Rosenwald J C 1994 On-axis and off-axis primary dose component in high energy photon beams *Med Phys* **21** 799-808

Zhu T C, Ahnesjö A, Lam K L, Li X A, Ma C M, Palta J R, Sharpe M B, Thomadsen B, Tailor R C and Group A T P C T 2009 Report of AAPM Therapy Physics Committee Task Group 74: in-air output ratio, Sc, for megavoltage photon beams *Med Phys* **36** 5261-91

Zhu T C and Bjarngard B E 1995 The fraction of photons undergoing head scatter in x-ray beams *Phys Med Biol* **40** 1127-34

Zhu X R, Kang Y and Gillin M T 2006 Measurements of in-air output ratios for a linear accelerator with and without the flattening filter *Med Phys* **33** 3723